# Planetary Wave Drag: Theory, Observation and its Role in Shaping the General Circulation

**Wim van Caspel**

A thesis submitted for the degree of
Master of Science, Climate Physics

*Supervisor:*
Dr. A.J. van Delden

**Utrecht University**

Institute for Marine and Atmospheric Research (IMAU)
Department of Physics

June 2018

# Abstract

Breaking planetary waves in the wintertime stratospheric surf-zone are associated with a local loss of angular momentum, or 'drag' force. This drag force is, among other things, responsible for driving the Brewer-Dobson circulation. The concept of planetary wave drag is investigated using zonal mean quasi-geostrophic theory. In particular, quasi-geostrophic potential vorticity is used to describe the coupled interactions between planetary waves, the polar vortex and the stratospheric surf-zone. Theory is complemented with observation using reanalysis data. To study the role of planetary wave drag in shaping the general circulation, a parameterization of planetary wave drag is implemented in a zonal mean model of the atmosphere. Results from quasi-geostrophic theory are used to interpret the model output. Model performance with respect to the observed climatology is quantified with the use of Taylor-diagrams. Furthermore, a selection of quasi-geostrophic results are tested and expanded upon using novel numerical cyclo-geostrophic piecewise PV-inversion experiments with Rossby-Ertel PV-configurations.

# Contents

# Chapter 1

# A look at the stratosphere

## 1.1 Introduction

This thesis sets out to provide an overview of the theory, observation and role of planetary wave drag in the general circulation. The theory forming the backbone of this work, largely revolves around the quasi-geostrophic approximation. Within quasi-geostrophic theory, planetary wave dynamics, as well as the large-scale dynamics of the stratosphere, can be studied in terms of a Potential Vorticity (PV) budget. The description of the dynamics surrounding planetary waves in terms of PV, lies at the heart of this work.

The contents of the first chapter are meant to serve as a general introduction to wintertime stratospheric dynamics, as well as to develop some of the 'tools' required for the subsequent chapters. In Ch. 2, a few fundamental properties and characteristics of planetary waves are discussed. These are then used in the description of planetary wave-mean flow interaction, in Ch. 3. The contents of Ch. 2 and 3 are supplemented by observation either directly in the text, or with reference to the animations shown in Appendix A.8. These animations are available upon request. In Ch. 4, the role of planetary wave drag is discussed within the framework of a zonal mean general circulation model. Model experiments are used to understand the role of planetary wave drag in shaping the general mean circulation. The model's parameterization of planetary wave drag and the model's output, is interpreted using the theory from Ch. 2 and 3.

Throughout this work, frequent comparisons of theory with observation as well as an emphasis on the most basic dynamics, is meant to give the reader an intuitive understanding of the dynamics which are involved with the concept of planetary wave drag. Reference is made to papers or books in which more rigorous derivations are given. To not obstruct the flow of the text, lengthier derivations and concepts which do not directly contribute to the narrative of planetary wave drag, are saved for the Appendix.

## 1.2 Wintertime dynamics and the polar vortex

Due to the tilt of Earth's axis of rotation with respect to its orbit around the sun, the Earth experiences seasons. The seasons are especially pronounced at high latitudes, where the difference between summertime and wintertime insolation is greatest. During wintertime, cooling increases the density of air, causing it to sink in accordance with hydrostatic balance. In the stratosphere, this leads to the formation of a robust low-pressure system centered over the wintertime pole. With radiative cooling being strongest at the pole, the low-pressure system becomes progressively weaker at lower latitudes. This effectively causes pressure surfaces to bulge downwards

towards the pole, giving them the shape of a bowl. Air generally tends to flow from high to low pressure areas, and because of the low-pressure system over the wintertime pole, air will want to flow towards the poles. However, because of the rotation of the Earth, conservation of angular momentum requires that the northward tendency of the wind due to the pressure gradient, is accompanied by an eastward Coriolis deflection. When the atmosphere is in geostrophic balance, which is generally a good approximation in the stratosphere, air will instead follow contours of constant geopotential height ($\phi$), defined by $\phi = -gz$, where $z$ is the Cartesian height of the pressure surface and $g$ is the acceleration due to gravity. Along a pressure surface, the geopotential height is indicative of the height of the pressure surface relative to the surface of the Earth. For the wintertime stratosphere, the bowl-shaped pressure surfaces can viewed as a succession of increasingly lower (circular) geopotential height contours. This causes the air to circle the wintertime pole, forming a giant polar vortex. This vortex, referred to as the stratospheric polar vortex, is fundamentally 'driven' by radiative cooling.

If the polar vortex is for whatever reason slowed down, geostrophic balance will be disrupted, and the pressure gradient force will induce poleward motion. In the presence of retrograde forces, the stratospheric polar vortex can then be viewed as trying to 'drain' into the North-pole's upper troposphere. To illustrate this metaphor, the geopotential height along the 50 hPa isobar is shown in Fig. 1.1. The arrows in Fig. 1.1 represent the direction and magnitude of the wind,

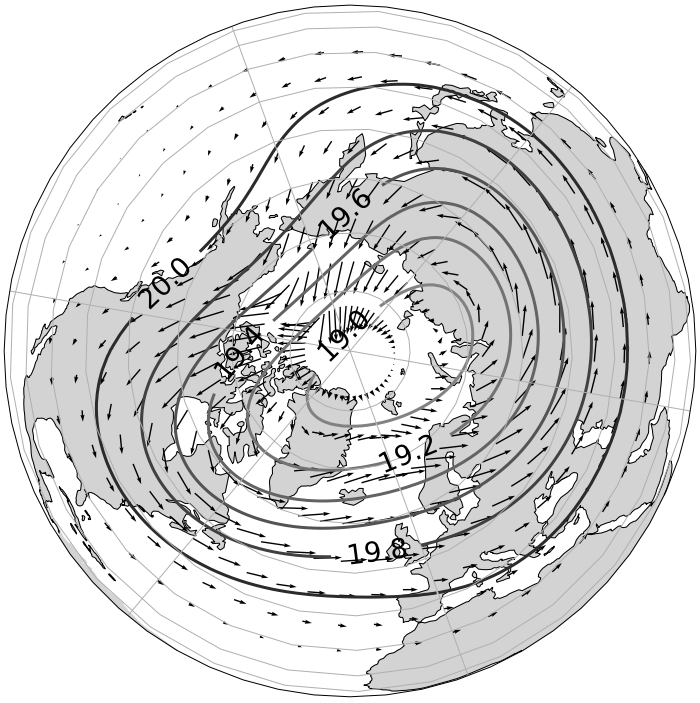


**Figure 1.1:** Stereographic projection of the 2010-2016 DJF mean values of the geopotential height (black contours) at 50 hPa, centered around the North pole. Contours are scaled by a factor of $10^{-5}$, arrows indicate the direction and magnitude of the isobaric wind. Largest arrows correspond to a wind speed of roughly 30 m/s. Data obtained from ECMWF ERA5 reanalysis (Appendix A.1).

with the largest arrows being on the order of 30 m/s. Towards the center of the vortex, the wind can be seen having a component which is not tangential to the geopotential height contours. This would not be possible if the flow is in perfect geostrophic balance, which alludes to the presence of turbulent motion and retrograde forces. For the latter, an intuitive candidate would be internal molecular viscous forces, but in the stratosphere these are negligible. As is hinted at

in the title of this work, this thesis explores the concept of breaking planetary waves providing the retrograde force responsible for the observed systematic northward component of the wind. The poleward tendency of the wind drives the so-called Brewer-Dobson circulation, which was named in honour of pioneering work done by Alan Brewer and Gordon Dobson in the middle of the 20th century. The systematic northward 'pumping action' by breaking planetary waves in the stratosphere, causes material tracers such as ozone to collect within the polar vortex. In addition to this, the high winds surrounding the vortex edge, located approximately between the 19.2e5 - 19.8e5 $m^2/s^2$ geopotential height contours in Fig. 1.1, act as a barrier, creating a marked difference between the composition of the interior and exterior of the vortex. This is especially relevant to the formation of the wintertime stratospheric ozone hole. Much of theory in discussed in this work, stems from research which was initiated by the need to understand the dynamics of the ozone hole.

In contrast to wintertime, the higher latitudes receive an abundance of solar radiation during summer. This effectively reverses the processes which lead to the formation of the wintertime polar vortex, and hence in summer a stratospheric high-pressure system with accompanying westward winds is observed. Due to dynamics discussed in Ch. 2 and 3, the dynamics surrounding planetary waves in the summertime stratosphere are however much less pronounced than those in wintertime. This gives, for example, the Brewer-Dobson circulation a strong seasonal character (Butchart [1]).

## 1.3 The quasi-geostrophic equations of motion

Conditions in the stratosphere are such that that the full equations of motion on a sphere, can be greatly simplified. Namely: (1) there is a high level of static stability, restricting vertical motion and making static stability only a function of height, (2) the Earth's rotation dominates the momentum balance, restricting meridional motion, (3) the horizontal length scale is much smaller than the radius of the Earth. For added convenience, an often employed method is to zonally average the entire system of equations. For any variable $a(x, y, z, t)$ the zonal average is denoted by an overbar, and is calculated as

$$\bar{a}(y, z, t) = \frac{1}{L} \int_0^L a(x, y, z, t) dx, \tag{1.3.1}$$

where $L$ is the length of the latitude circle at $y$ and where the $(x, y, z)$-coordinates span a Cartesian grid. In addition to zonally averaging, variables can be split in a zonal mean and eddy term as follows,

$$a(x, y, z, t) = \bar{a}(y, z, t) + a'(x, y, z, t). \tag{1.3.2}$$

This definition of eddies, or zonal asymmetries, therefore depends fundamentally on the definition of the zonal mean. The power of Eq. 1.3.1 lies in the fact that it allows for the 'natural' decomposition of the general circulation in a primary zonal circulation, a secondary meridional circulation, and eddies in the form of zonal asymmetries. Note that by the definition of Eq. 1.3.2, it follows that $\overline{a'}(x, y, z, t) = 0$. As a final simplification, the often employed method of a $\beta$-plane approximation is used. This approximation was first published by Carl-Gustav Rossby in the early 20th century, and it assumes the mid-latitude background planetary vorticity gradient to vary linearly. Around a certain latitude, usually taken to be $y_0$ at 45 degrees north, the Coriolis parameter is then written as

$$f = f_0 + \beta(y - y_0). \tag{1.3.3}$$

Here $y$ is the meridional coordinate and $f_0$ is the Coriolis parameter at $y_0$. The $\beta$-plane parameter is defined as $\beta = 2\Omega a^{-1}\cos(\phi_0)$, where $\Omega$ and $a$ are the Earth's angular velocity and radius, respectively.

Geostrophic flow is non-divergent, which allows for the geostrophic components of the wind to be written in terms of the geostrophic stream function ($\psi$). The geostrophic stream function $\psi = p/f_0\rho_0$, is defined such that the geostrophic velocity field is given by $(u, v) = (-\partial_y\psi, \partial_x\psi)$, and that the buoyancy force is given by $b' = f_0\partial_z\psi$. Using the quasi-geostrophic scaling arguments on a $\beta$-plane, zonally averaging, and with the definition of the zonal mean and eddy terms, the quasi-geostrophic equations of motion are written as[1]

$$\frac{\partial\bar{u}}{\partial t} - f_0\bar{v_a} = \mathcal{G}_x - \frac{\partial}{\partial y}\overline{u'v'} \tag{1.3.4a}$$

$$\frac{\partial\bar{v_a}}{\partial y} + \frac{\partial\bar{w_a}}{\partial z} = 0 \tag{1.3.4b}$$

$$f_0\frac{\partial}{\partial z}\bar{u} = -\frac{\partial}{\partial y}\bar{b} \tag{1.3.4c}$$

$$\frac{\partial\bar{b'}}{\partial t} + \bar{w_a}N^2 = \mathcal{B} - \frac{\partial}{\partial y}\overline{v'b'}. \tag{1.3.4d}$$

Here $(\bar{v_a}, \bar{w_a})$ is the second order ageostrophic velocity, $N^2$ is the square of the buoyancy frequency defined in QG-theory by $N^2 = \partial_z\bar{b}$, and $\mathcal{G}_x$ and $\mathcal{B}$ are external momentum and buoyancy forcings, respectively. The buoyancy field is defined as $b = \bar{b}(z) + b'(x, y, z, t)$, where $\bar{b}$ is the basic state buoyancy. The buoyancy force $b'$ is defined as $b' = -g(\rho'/\rho)$, or equivalently as $b' = g(\theta'/\theta)$, where $\rho$ and $\theta$ are the density and potential temperature, respectively. From top to bottom, Eq. 1.3.4a is the zonal momentum budget, Eq. 1.3.4b the continuity equation, Eq. 1.3.4c describes thermal wind balance and Eq. 1.3.4d is the thermodynamic equation. The latter depends on the fact that $w_a$ only advects the basic state buoyancy $\bar{b}$.

The perturbation terms $(u', v') = (-\partial_y\psi', \partial_x\psi')$, represent eddy terms of the first-order geostrophic stream function. These eddy terms are independent of the ageostrophic circulation, and by Eq. 1.3.1, need not be small. These eddy terms are therefore of an higher order than the ageostrophic velocities that drive the residual circulation. One of the key features of Eq. 1.3.4a - Eq. 1.3.4d, is that the time-development of the flow is completely captured by the quantity called Quasi-Geostrophic Potential Vorticity (QGPV). The QGPV ($q$) is defined in terms of the geostrophic stream function as

$$q = \nabla^2\psi + f + \frac{f_0^2}{\rho}\frac{\partial}{\partial z}\left(\frac{\rho}{N^2}\frac{\partial\psi}{\partial z}\right) \tag{1.3.5a}$$

$$\frac{D_g q}{Dt} = \chi. \tag{1.3.5b}$$

In Eq. 1.3.5b, $D_g/Dt$ represents the geostrophic material derivative defined by $D_g/Dt = \partial_t + u_g\partial_x + v_g\partial_y$, and $\chi$ represents sources and sinks of $q$, such as friction and diabatic processes. The geostrophic subscript on the velocity terms is often dropped, to write $(u_g, v_g) = (u, v)$. When there are no non-conservative effects, i.e. $\chi = 0$, this corresponds to $\mathcal{G}_x = \mathcal{B} = 0$. The terms on the right-hand side of Eq. 1.3.5a represent geostrophic relative vorticity, planetary vorticity defined by Eq. 1.3.3, and a 'stretching' term, respectively. Note that for the relative vorticity, it follows from the definition of $\psi$ that $\zeta_g = \nabla^2\psi = (\partial_x v - \partial_y u)$. From Eq. 1.3.5b it follows

[1] A step-by-step derivation of the Quasi-Geostrophic (QG) equations of motion is available in many books on geophysical fluid dynamics, e.g. Vallis [2] Ch.5, or in log-pressure coordinates in Andrews *et al.* [3] Ch.3.

that for conservative flows ($\chi = 0$), $q$ is a conserved quantity following horizontal geostrophic motion. Splitting the variables for a conservative flow in a mean and eddy term as before, and taking the zonal mean, reduces Eq. 1.3.5b to

$$\frac{\partial \bar{q}}{\partial t} + \frac{\partial}{\partial y}\overline{v'q'} = 0. \tag{1.3.6}$$

This expression relies on the fact that, (1) terms containing zonal derivatives vanish with zonal averaging, (2) zonal means of perturbation terms vanish by the definition of Eq. 1.3.2, (3) geostrophic flow is non-divergent, such that $\partial_y \bar{v'} = 0$. Normally, the non-divergent geostrophic flow is augmented by the ageostrophic circulation to ensure mass conservation. The result of Eq. 1.3.6 is therefore a bit counter-intuitive in the sense that the complete time development of the zonal mean flow, which also includes the ageostrophic velocities, is determined only by the geostrophic meridional eddy fluxes of $q$.

The quasi-geostrophic approximation essentially filters small-scale dynamics from the equations of motion, which is why it is so well suited for modelling the dynamics of the stratosphere. What remains is a flow in which the pressure gradient and Coriolis force are almost exactly in balance, with 'quasi' referring to the inclusion of second-order inertia effects. This implies that small-amplitude waves such as inertio-gravity and gravity waves cannot be represented by QG-theory, but these waves typically only play a role at altitudes much higher than the stratosphere (e.g. Holton [4]). In the context of this thesis, the most important property of QG-theory, is that the QGPV-budget entirely governs the time development of the flow. This allows for a 'PV-view' of the dynamics, in the knowledge that it directly translates to the dynamics governed by the full equations of motion given by Eq. 1.3.4a - 1.3.4d. It should be noted that QG-theory is rather a rough approximation, with a more complete description of PV-dynamics being given by the 'exact' Rossby-Ertel PV, often simply referred to as PV in isentropic coordinates. However, the qualitative insights given by QG-theory are robust, in the sense that more sophisticated models do not have fundamentally different large-scale dynamics.

To conclude, QG-theory allows for a 'PV-view' of the large-scale dynamics in the stratosphere. Rossby-Ertel PV dynamics may refine this picture, but the large-scale features are still qualitatively similar to those from QG-theory. This notion lies at the core of the first three chapters of this thesis, as it justifies the study of the stratosphere in terms of (QG)PV.

## 1.4 PV-maps and PV-inversion

Throughout this work, direct observations are often graphically displayed using isentropic Potential Vorticity maps (PV-maps). These maps have a number of properties which can help with the interpretation of the observed dynamics, as is argued in detail by Hoskins *et al.* [5]. There are two main properties which stand out. The first is that Rossby-Ertel PV ($Z$), here referred to simply as PV, is a conserved quantity following adiabatic and frictionless motion along isentropic surfaces. In isentropic $(x, y, \theta)$-coordinates, $Z$ is defined as

$$Z = \frac{\xi_\theta + f}{\sigma}, \tag{1.4.1}$$

where $\sigma$ is the isentropic density defined by $\sigma = -g^{-1}\partial_\theta p$, $f$ is the Coriolis parameter, and $\xi_\theta = \nabla \times (u_\theta, v_\theta)$ is the relative isentropic vorticity. Conditions in the stratosphere are such that, to good approximation, the flow is frictionless and adiabatic on the time scale of about two weeks. This is roughly equivalent to the time scale of planetary wave breaking, which allows for the use of $Z$ as a tracer following wave breaking motion from observation.

Taking into account that the background planetary vorticity ($f$) dominates the PV-budget, a clear positive South-to-North PV-gradient is usually visible on PV-maps. This makes it so that meridional displacement of air is easily distinguishable. For example, southward displacement will lead to a intrusion of high PV air into a region of relatively low PV. In the context of this thesis, this is particularly relevant because planetary waves tend to consistently mix PV down-gradient, i.e. from North to South (section 2.4). The latest reanalysis product of ECWMF (ERA5, Appendix A.1) natively interpolates to a 0.3-by-0.3 degree grid, and provides data at hourly intervals. This results in PV-maps with a high amount of detail, as is demonstrated in Fig. 1.2, where the PV-field on the 850K isentrope over the time span of two days is shown. Supplementary animations of the time development of the PV-field over the entire Northern hemisphere can be found in Appendix A.8. PV-maps, and especially animated PV-maps, can provide valuable insight on much of the planetary wave dynamics discussed in Ch. 2 and 3.

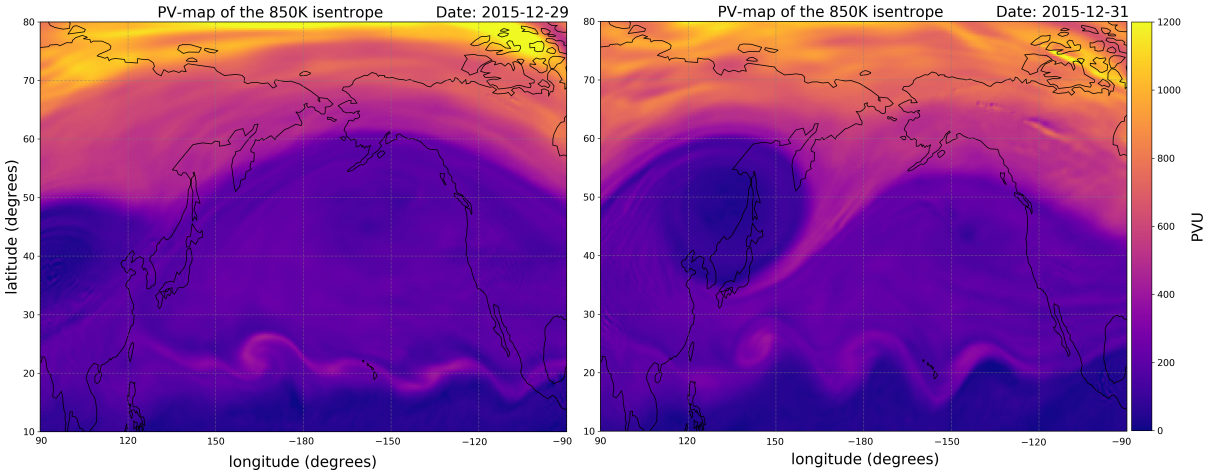


**Figure 1.2:** PV-maps of the 850K isentrope over the Pacific ocean. Left panel: instantaneous PV-field on 2015-12-28 00:00 hrs. Right panel: instantaneous PV-field on 2015-12-30 00:00 hrs. PV is expressed in Potential Vorticity Units (1 PVU = $10^{-6}$ K m$^2$ kg$^{-2}$ s$^{-1}$). Data retrieved from ECMWF ERA5 reanalysis (Appendix A.1).

The second important property of PV-maps, ties in with a cornerstone of the 'PV-view' discussed in section 1.3, namely that of the PV-invertibility principle. The principle of PV-inversion states that all dynamical fields can be reconstructed from the PV-distribution, using a balanced assumption. Thus, PV-inversion links, for example, the pressure, velocity and temperature field to the instantaneous PV-distribution, by inverting a function of the form

$$E(u, v, p, \theta, \dots) = Z(x, y, \theta). \tag{1.4.2}$$

A conceptually powerful aspect of PV-inversion, is that it connects changes in the distribution of PV to changes in the distribution of (angular) momentum. This is an important notion in terms of planetary wave drag, i.e. angular momentum loss, because planetary waves are principally investigated in terms of their induced fluxes of (QG)PV. An important aspect of PV-inversion is that it requires appropriate boundary conditions for the inversion to be unique. The 'resolution' of the inversion depends largely on the restrictions imposed by the balanced assumption. For example, the quasi-geostrophic assumptions are pretty 'rough', and hence PV-inversion with the use of QGPV, results in relatively coarse inverted fields. More accurate methods for PV-inversion revolve around using the 'exact' Rossby-Ertel PV.

# Chapter 2

# Planetary waves

Planetary waves, often referred to as Rossby waves, are waves in the oceans and atmosphere which exist fundamentally due to a vorticity gradient. The strong pole-to-pole vorticity gradient imposed by the counter-clockwise rotation of the Earth, makes it so that planetary waves are prevalent in the Earth's ocean and atmosphere. Planetary waves tend to reside where the vorticity gradient is strongest. Tying in with this notion, is that the stratospheric polar vortex edge is associated with a high vorticity gradient. Planetary waves therefore prefer to reside on the polar vortex edge. There they play an important role in governing the dynamics surrounding the polar vortex, which also impact the dynamics of the stratosphere as a whole. Indeed, planetary waves arguably underpin all of the most dominant dynamical features of the wintertime stratosphere (e.g. Plumb [6] for a discussion).

Earth's monotonically increasing South-to-North background potential vorticity distribution, gives planetary waves a set of peculiar 'one-way' properties. For example, planetary waves can only propagate westward relative to the background flow, and never eastward. The one-way nature of some of the properties of planetary waves, lies at the heart of the concept of planetary wave drag. In this chapter, the focus lies on describing these wave properties, as well as on describing some of the general characteristics of the waves. This will be done mostly in terms of results from quasi-geostrophic theory. However, only in chapter 3 will quasi-geostrophic theory be used to explicitly describe the interaction between planetary waves and the mean flow.

## 2.1 Shallow water $\beta$-plane dynamics

This section concerns perhaps the simplest manifestation of planetary waves, namely that of a zonally propagating planetary wave in a shallow water $\beta$-plane channel. The main goal of this section is to introduce the concept of planetary wave elasticity, and to show how quasi-geostrophic planetary waves can be associated with zonal mean meridional eddy fluxes of QGPV ($q$, Eq. 1.3.5a).

In a motionless atmosphere, the background planetary vorticity gradient will make it so that PV-contours lie along latitude circles. Planetary waves are expressed as undulations of these otherwise 'straight' contours. As argued in Ch. 7 from Dijkstra [7], for a constant layer depth $H$ and variable $\beta$-plane Coriolis parameter $f$, the shallow water $\beta$-channel PV ($\tilde{q}$) can be used to describe the mechanism of horizontal planetary wave propagation. The expression for $\tilde{q}$ is given by

$$\tilde{q} = \frac{\xi + f}{H}, \tag{2.1.1}$$

where $f$ is as in Eq. 1.3.3, and $\xi$ is the relative vorticity. Note that $\xi = 0$ for a motionless layer

of fluid, and that counter clock-wise rotation of fluid parcels is associated with positive $\xi$, and clock-wise rotation with negative $\xi$. Per usual, $\tilde{q}$ is a conserved quantity for conservative flows ($\chi = 0$ as in Eq. 1.3.5b).

Consider a section of a shallow water $\beta$-plane, centered around the latitude $y_0$. In a motionless state, the PV-contour $\tilde{q}(y_0)$, which corresponds to the background planetary vorticity at $y_0$, will lie along the $y_0$-axis, as depicted by the dotted grey line in Fig. 2.1. If a planetary

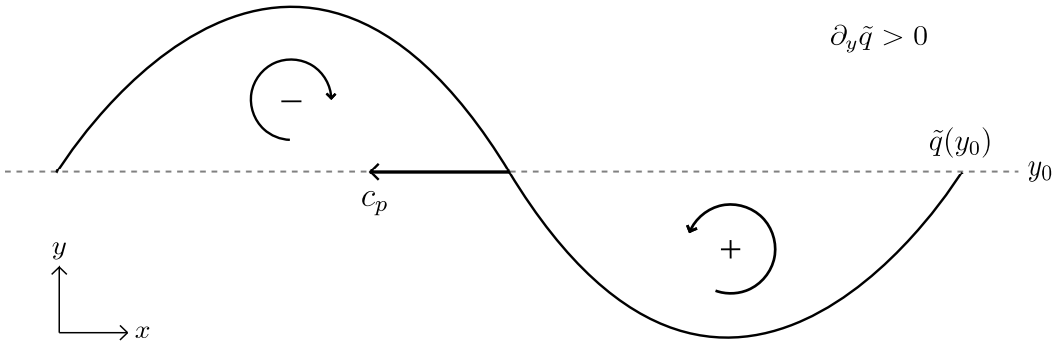


**Figure 2.1:** One period of a planetary wave in a shallow water $\beta$-channel with constant layer depth $H$, centered around $y_0$. The dotted line corresponds to the PV-contour $\tilde{q}(y_0)$ for a state of rest, the black line to the PV-contour after a planetary wave is introduced. Meaning of the symbols is explained in the text, PV is described by Eq. 2.1.1.

wave is introduced, the PV-contour will deform, taking on the shape of the solid black line in Fig. 2.1. With a positive background PV-gradient ($\partial_y \tilde{q} > 0$) as well as PV being conserved, a northward undulation of the PV-contour will displace fluid with relatively low PV to a region of relatively high PV. This creates a negative PV-anomaly with respect to the background PV-distribution. Likewise, a southward undulation will create a positive PV-anomaly. With Eq. 2.1.1, the effects of a PV-anomaly can be understood as a change in relative vorticity: If the fluid was initially at rest, i.e. $\xi = 0$, a northward displacement of a fluid parcel will induce negative relative vorticity to compensate for the increase in $f$. This relation follows from the conservedness of $\tilde{q}$ and the numerator of Eq. 2.1.1. Similarly, $\xi$ must become positive wherever the PV-contour undulates southwards. The velocity fields associated with the induced relative vorticity fields, are drawn inside the ridge and trough of the wave in Fig. 2.1. In the middle of Fig. 2.1, where $\tilde{q}(y_0)$ intersects the $y_0$-axis, the velocity fields can be seen to conspire to 'push' the black contour down. If the wave is imagined to extend beyond the domain drawn in Fig. 2.1, it can be seen that the induced velocity fields conspire to push the contour up along the left and rightmost $y_0$-intersections drawn in Fig. 2.1. This mechanism effectively pushes the wave down wherever the zonal derivative of the PV-contour is negative, and up wherever it is positive. This combined pushing action, makes it so that the wave propagates westward. This is based on the analysis of the induced relative vorticity fields, whose orientation and strength depends on the background vorticity gradient. It is then a consequence of the positive South-to-North planetary background PV-gradient, that planetary waves propagate westward. This implies that their zonal phase speed $c_p$ is always negative, which is marked by the arrow in Fig. 2.1. The negative definite sign of $c_p$ is reflected in the expression for the dispersion relation of planetary waves on a motionless horizontal flow (e.g. Vallis [2] section 6.4.2), given by

$$\omega = -\beta \frac{k}{k^2 + l^2}, \tag{2.1.2}$$

where $k$ and $l$ are the longitudinal and latitudinal wavenumber, respectively. With the definition of $k = 2\pi/\lambda$, where $\lambda$ is the longitudinal wave length, and the analogous definition of $l$, $k$ and $l$

are always positive. Note that the dependence of Eq. 2.1.2 on $\beta$ demonstrates that planetary waves owe their existence to a (planetary) vorticity gradient. The zonal phase speed of waves is defined by $c_p = \omega/k$, which for planetary waves, using Eq. 2.1.2, follows as

$$c_p = -\frac{\beta}{k^2 + l^2}. \tag{2.1.3}$$

By the definitions of $\beta$, $k$ and $l$, $c_p$ is always negative, which is in accordance with the propagation mechanism described by Fig. 2.1. The notion of westward propagation extends to waves imposed on a constant zonal flow. For such flows, $\partial_y u = 0$, and hence relative vorticity is unaffected. The described restoring mechanism, which operates in terms of the induced relative vorticity fields, then also remains unaffected. A more general notion would therefore be that planetary waves can only propagate westward with respect to the background zonal flow. A consequence of this is that, if the background zonal wind is more eastward than the wave's phase speed is westward, an observer on the surface of the Earth will be able to see a planetary wave propagate eastward.

From the role of the relative vorticity fields in planetary wave propagation, it can be understood that relative vorticity essentially 'drives' the waves' propagation mechanism. The strength of the induced relative vorticity fields depends on the strength of the background (planetary) vorticity gradient, in the same way that $\xi$ depends on $f$ in Eq. 2.1.1. Thus, on a high PV-gradient, the 'PV restoring mechanism' is greatest. The restoring mechanism inhibits the tendency of the PV-contours to deform: It is as if the contours are strung tighter on a high PV-gradient. In literature this is referred to as the elasticity of the PV-contours, or equivalently, as 'planetary wave elasticity' (e.g. Baldwin *et al.* [8]). Planetary wave elasticity is relatively high on the high PV-gradient associated with the polar vortex edge. This increases the resilience of the polar vortex edge, leading to the persistence of its structure. An example of numerical planetary wave elasticity experiments, or 'barrier-penetration experiments', can be found in section 3 of Dritschel and McIntyre [9].

To demonstrate the connection between planetary waves and zonal mean meridional fluxes of QGPV, consider a shallow water quasi-geostrophic wave developing from an initially straight QGPV-contour as in Fig. 2.2. It should be noted that the single layer expression for QGPV

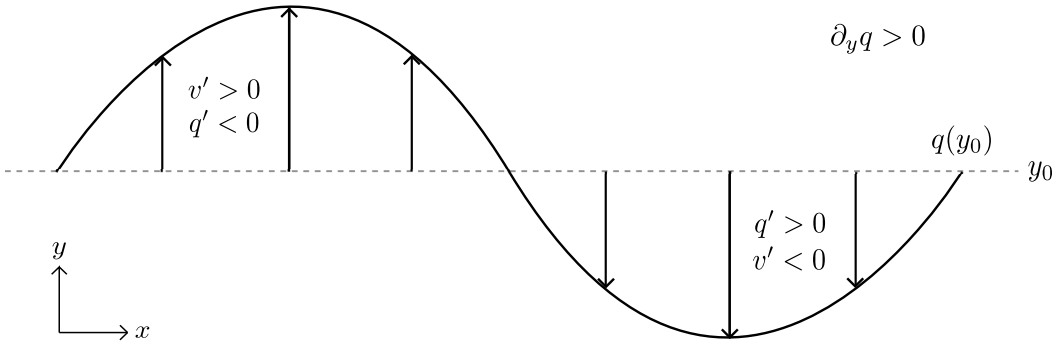


**Figure 2.2:** One period of a planetary wave in a quasi-geostrophic shallow water $\beta$-channel, centered around $y_0$. The dotted line corresponds to the QGPV-contour $q(y_0)$ for a state of rest, the black line to the QGPV-contour after a planetary wave is introduced. Arrows indicate meridional displacement of the QGPV-contour as the wave develops.

is not equivalent to Eq. 2.1.1. The single layer QGPV can be derived by applying the quasi-geostrophic approximation to Eq. 2.1.1, and its expression will appear in an example in section 3.2. As before, the black line in Fig. 2.2 represents an undulation of the dotted grey contour corresponding to the QGPV-distribution of an initially motionless state. Because QGPV is

conserved, the QGPV-contour represents a material contour. If a material contour is to be displaced meridionally, this can only be achieved through advection by a meridional component of the wind. In QG-theory, QGPV is only advected by the geostrophic wind. Meridional displacement of a material contour of QGPV, can then only be achieved through a non-zero component of the geostrophic meridional wind[1], $v'$. If the PV-contour is displaced northward, $v' > 0$, and if it is displaced southward, $v' < 0$. Because of the positive background QGPV-gradient, negative and positive PV-anomalies will form in the ridge and trough of the wave, respectively. Inside the ridge of the wave, $q$ is lower than the zonal mean $\bar{q}$, and hence $q' < 0$. Likewise, in the trough of the wave, $q$ is higher than the zonal mean $\bar{q}$, and hence $q' > 0$. For a wave developing from the initially horizontal QGPV-contour, the corresponding signs of $v'$ and $q'$ are drawn inside the trough and ridge shown in Fig. 2.2. The significance of these eddy terms, lies in the observation that the multiplication of $v'$ with $q'$ is always negative. This applies also to the zonal mean of the eddy product, such that $\overline{v'q'} < 0$ when a wave develops as in Fig. 2.2. If the solid black line drawn in Fig. 2.2 would return back to its original state, i.e. the dotted grey-line, the sign of the $v'$ terms will reverse. The sign of $q'$ will however remain the same. After all, the sign of $q'$ corresponds to the sign of the QGPV-anomaly, which does not depend on whether the anomaly is growing or diminishing. The sign of the eddy product $v'q'$ will then be everywhere positive. 'Leaving' planetary waves, can therefore be associated with $\overline{v'q'} > 0$.

In terms of a zonal mean 'PV-view' of the atmosphere, the relation between eddy fluxes of $\overline{v'q'}$ and the development of planetary waves turns out to be an important notion, which will be further elaborated upon in Ch. 3. There, eddy fluxes of $\overline{v'q'}$ will be shown to relate to a zonal force as well as the time development of zonal planetary wave activity in a stratified atmosphere. Adding to the pivotal role of eddy fluxes of QGPV, is that in zonal mean QG-theory, changes in the zonal mean QGPV-distribution can only be brought about by eddy fluxes of $\overline{v'q'}$, as is determined by Eq. 1.3.6. To aid the discussion in section 2.4, the Taylor-identity for a quasi-geostrophic shallow water $\beta$-plane (the 'full' identity will be discussed in section 1.3), is written as

$$\overline{v'q'} = -\frac{\partial \overline{u'v'}}{\partial y}. \tag{2.1.4}$$

The right-hand side of Eq. 2.1.4 corresponds to a zonal force by virtue of its appearance in the zonal momentum budget given by Eq. 1.3.4a. The undulation of the PV-contour in Fig. 2.1 can then, by the sign of the corresponding negative eddy fluxes of $q$, be associated with a westward zonal force by Eq. 2.1.4. The discussion surrounding Fig. 2.1 is an informal example of the relation between $\overline{v'q'}$ and planetary wave activity, considering only a single layer of fluid. However, in the description surrounding Fig. 2.1, a distinction should be made between a planetary wave entering the layer and the wave being forced within the layer. Generally speaking, if a wave is forced somewhere, it will propagate away from this region. In addition to the horizontal propagation mechanism discussed in this section, it will be discussed how planetary waves can propagate vertically in section 2.2. Either way, planetary waves will generally be leaving the region where they are forced, such that $\overline{v'q'} > 0$ is typical of planetary wave 'source' regions.

[1]The meridional geostrophic velocity ($v$) and QGPV ($q$) are split in a zonal mean and eddy term as $v = \bar{v} + v' = \overline{\partial_x \psi} + v' = v'$ and $q = \bar{q} + q'$.

## 2.2 Vertical propagation

Planetary waves are typically forced within the troposphere by baroclinic instability, orography and land-sea temperature contrasts[2], with the strongest forcing occurring at roughly 60 degrees North (or 60 degrees South for the Southern Hemisphere). In the context of this thesis, the focus lies on planetary waves in the stratosphere. It follows then that the waves are able to propagated vertically. The conditions under which vertical propagation can occur, as well as the manner in which the waves do so, are discussed in this section.

A classic result in wave mean flow theory is the so-called Charney-Drazin criterion, published in 1961 by Charney and Drazin [10], which puts a constraint on when planetary waves can propagate vertically. For a constant background zonal wind $\bar{u}$, the (quasi-geostrophic) Charney-Drazin criterion reads

$$0 < \bar{u} < \frac{\beta}{k^2 + l^2 + (f_0/2NH)^2}. \tag{2.2.1}$$

Here $N$ is the buoyancy frequency, $H$ is the vertical scale height (typically taken to be 8km), and the other terms are as before. The first condition from Eq. 2.2.1 requires that the zonal mean winds be positive, i.e. to the east, for planetary waves to propagate vertically. This condition plays an important role in shaping the difference between the summer and wintertime stratosphere. During summer, the upper tropospheric and lower stratospheric winds are westward for reasons discussed in section 1.2, such that planetary waves cannot propagate upward. Consequently, the summer polar vortex is much more devoid of planetary waves compared to its wintertime counterpart. The second condition from Eq. 2.2.1, implies that when the zonal winds are too strong, upward propagation is also inhibited. The 'cut-off' speed is higher for longer planetary waves, which follows from the denominator of Eq. 2.2.1. Here 'longer' refers to the zonal wavelength, which is the most relevant measure of planetary wavelength in the context of this thesis. For a purely zonal wave, $l = 0$. Assuming the term $(f_0/2NH)^2$ from Eq. 2.2.1 to be constant, the upper bound on $\bar{u}$ is only determined by $k$. With the definition of $k = 2\pi/\lambda$, where $\lambda$ is the zonal wavelength, it follows that the right-most term in Eq. 2.2.1 is largest for longer waves.

During wintertime, zonal winds generally increase with altitude. This is related to thermal wind balance (Eq. 1.3.4c), which states that a negative meridional temperature gradient (caused by radiative cooling) induces a positive vertical shear of the zonal wind. For all but the longest planetary waves, this causes the 'cut-off' zonal wind speed prescribed by Eq. 2.2.1, to be reached at a certain altitude. This effect can be observed in the vertical isentropic cross-section of the atmosphere between 370K and 850K, shown in Fig. 2.3. In this figure, planetary wave-numbers can be identified by counting the number of troughs and ridges lying along a latitude circle and sharp vorticity gradient. From top left to bottom right, (1) at 370K, there exist planetary waves in the range of wave-number 3 to 5, (2) at 430K, wavenumber 5 has been filtered and wavenumber 3 is most distinguishable, (3) at 600K only wavenumber 2 is distinguishable, (4) at 850K there is only a single trough centered over the Aleutian Low, implying that all but wave-number 1 has been filtered. The edge of the polar vortex coincides with the maximum of the zonal winds, which will be discussed in terms of a 'PV-view' in section 3.3. The strong winds along the vortex edge, act as a 'window' through which only the longest planetary waves can propagate, because the shorter waves get filtered. In the Southern Hemisphere (SH), transient waves, which generally have a relatively high wavenumber, are more important than in the NH (e.g. Scinocca and Haynes [11]). Or rather, because of the unobstructed Southern Ocean, there is a lack of

[2]Orography and land-sea temperature contrasts are frequently bundled as 'topographic forcings'.

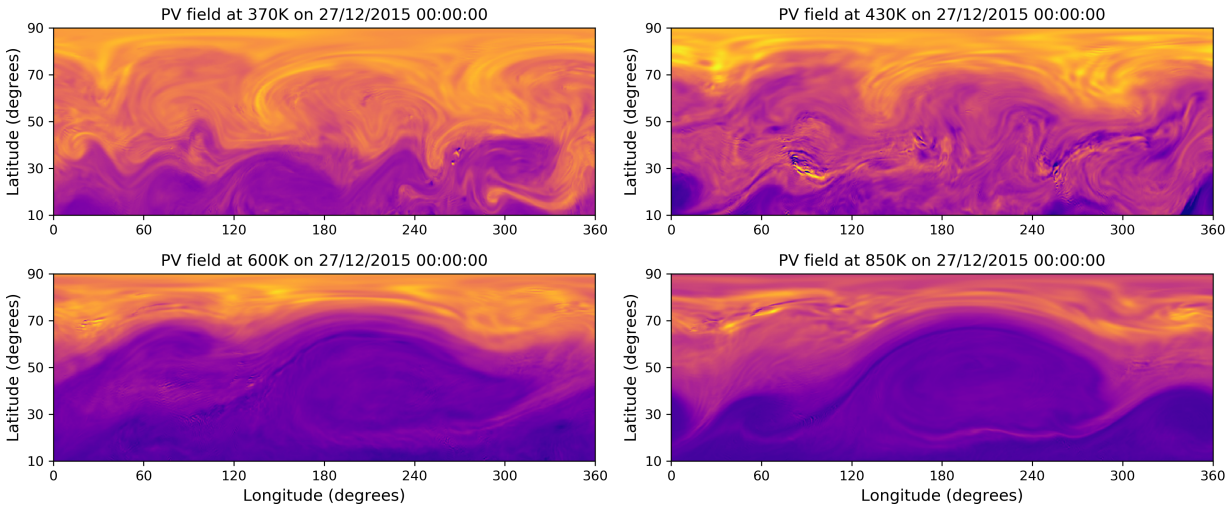


**Figure 2.3:** PV-maps ranging from 370K to 850K with no particular scaling, showing a vertical cross-section of the atmosphere on the 27th of December, 2015. Data retrieved from ECMWF ERA5 reanalysis (Appendix A.1). Animations of the wintertime (DJF) months along eight isentropic levels between 370K and 850K are available in Appendix A.8, Fig. A.10.

long stationary topographically forced planetary waves. Because the shorter baroclinically forced waves cannot propagate up into the stratosphere so easily, the SH wintertime stratospheric polar vortex is typically more devoid of planetary waves compared to its NH counterpart.

The Charney-Drazin criterion puts a constraint on when planetary waves can propagate vertically, but it does not say anything about the manner in which the waves do so. One of the perhaps more obvious factors affecting vertical propagation, is the exponentially decreasing density with height. Because of this decrease in density, the wave amplitude can be expected to grow exponentially as a function of height (e.g. Hoskins and James [12] Ch. 18.6). The linear description of planetary waves, which is an often employed method, assumes the amplitude of the waves to be small. If the waves propagate upward and grow in amplitude, this makes it so that linear theory will at some point become inadequate, and that non-linear dynamics become important. This notion is especially relevant to the discussion on wave breaking in section 2.4. In addition to growing in amplitude with height, planetary waves also tend to bend equatorwards with height (e.g. Matsuno [13]).

In QG-theory, the vertical eddy momentum fluxes induced by vertically propagating planetary waves is, rather counter-intuitively, proportional to a meridional eddy heat flux. Vertically propagating planetary waves induce deformations of stratification surfaces, which gives rise to the concept of 'form stress', discussed in Appendix A.4. The vertical planetary wave induced momentum flux per unit mass, is given by the expression

$$\frac{f_0}{N^2}\overline{v'b'}. \tag{2.2.2}$$

The buoyancy force $b'$ is by definition proportional to a density perturbation, or equivalently, a temperature perturbation. Eq. 2.2.2 can therefore be expressed in terms of an eddy flux of heat, meaning that the vertical eddy momentum flux is proportional to $\overline{v'\theta'}$, where $\theta$ is potential temperature. How this corresponds to a vertical momentum flux, follows from the analysis in Appendix A.4. The derivation of Eq. 2.2.2 given therein, can be summarized as follows: A vertical perturbation of a pressure surface is proportional to a buoyancy perturbation, and hence also to a temperature perturbation. A vertical buoyancy perturbation in turn induces a zonal

pressure perturbation $\partial_x p'$. This pressure perturbation is proportional to $v'$ through geostrophic balance, which states that $\partial_x p = f_0 \rho_0 v$. The coupling of a vertical pressure perturbation with a buoyancy perturbation, and of a zonal pressure perturbation with $v'$, makes it so that the vertical eddy momentum flux is proportional to a meridional eddy buoyancy (or heat) flux. Note that by the definition of $f_0$, $N^2$ and $b'$, the dimension[3] of the expression in Eq. 2.2.2 is $m^2 s^{-2}$. This is equivalent to the dimension of the horizontal wave induced eddy momentum flux $\overline{u'v'}$, which will be discussed in section 3.1. The description of how planetary wave induced eddy momentum fluxes tie in with planetary wave dynamics, requires the concepts of planetary wave activity and the Eliassen-Palm vector, which will be discussed in sections 2.3 and 3.1, respectively.

## 2.3 Pseudomomentum and momentum transport

Pseudomomentum ($\mathcal{M}$) is a property of waves, and in the context of this thesis, it relates to the momentum transport by planetary waves. However, pseudomomentum and momentum are not the same thing. Pseudomomentum is, by definition, a wave property which is invariant under spatial translation of the wave in a homogeneous medium. This makes it an abstract concept, but luckily the quasi-geostrophic (second-order) expression for pseudomomentum takes on a relatively simple form. Namely, it is proportional to the zonal pseudomomentum density defined in Eq. 2.3.3, which will be further elaborated on in this section. The interaction between planetary waves and the mean flow, make it look 'as if' the waves have momentum equal to their pseudomomentum. At the center of this section, lies the notion that zonal planetary wave pseudomomentum is negative definite when the background PV-gradient is positive, as is the case on Earth. It is then 'as if' planetary waves can only have negative zonal momentum. This makes it so that the waves can only transport negative zonal momentum away from their source region, and towards the region where they dissipate. In Appendix A.2, the concept of pseudomomentum is discussed in some more detail with a graphical illustration.

Hamiltonian dynamics revolve around the study of conserved quantities. When PV is conserved, pseudomomentum is by definition a conserved quantity, and hence its description, or derivation, is set within the framework of Hamiltonian dynamics. In the context of geophysical fluids, a review of Hamiltonian dynamics is given in the chapter on Dynamical Meteorology, published in the Encyclopedia of Atmospheric Sciences [14]. One of the results described therein, is for the pseudomomentum of planetary waves in a barotropic flow on a $\beta$-plane. Planetary waves are expressed as disturbances to a general 'basic state' PV-distribution ($q_0$). In the context of Fig. 2.1 in section 2.1, the basic state would be the background planetary vorticity gradient, and the wave-induced PV-anomalies would be the disturbances. For a zonally symmetric basic state and the function $Y$ defined by $Y(q_0(y)) = y$, where $q_0$ is a monotonically increasing basic state PV, the barotropic pseudomomentum is given by (Eq. 47 p. 329 of [14])

$$\mathcal{M} = \iint \left\{ -\int_0^{q-q_0} \left[ Y(q_0 + \tilde{q}) - Y(q_0) \right] d\tilde{q} \right\} dxdy. \tag{2.3.1}$$

Here the upper integration limit $q - q_0$ represents the local deviation from the basic state PV-distribution, which corresponds to the local magnitude of the wave-induced PV-anomalies. To determine the sign of $\mathcal{M}$, consider the following: If at some point in the $(x, y)$-domain $q - q_0 < 0$, the term $\tilde{q}$ is less than or equal to zero over its integration range, implying that also $q_0 + \tilde{q} \leq q_0$

[3]The dimensions of the buoyancy force, buoyancy frequency and planetary vorticity are given by $b' = -g\rho'/\rho$ $[m/s^2]$, $N^2 = \partial_z \bar{b}$ $[1/s^2]$ and $f_0 = 2\Omega \sin \phi_0$ $[1/s]$, respectively.

and hence $Y(q_0+\tilde{q}) \leq Y(q_0)$ over the integration range, by the definition of $Y$. This will make it so that the term $\left[Y(q_0+\tilde{q})-Y(q_0)\right]$ is always less than or equal to zero over the integration interval $[0,\, q-q_0]$. If at some point in the domain $q-q_0>0$, the reverse is true, such that $\tilde{q}$ is greater or equal to zero and corollary $\left[Y(q_0+\tilde{q})-Y(q_0)\right]$ is also greater than or equal to zero. This makes the integral over $d\tilde{q}$ in Eq. 2.3.1 always evaluate to a non-negative value, in the same way that for example, $\int_0^a x dx$ is positive for any non-zero real value of $a$. The integrand in Eq. 2.3.1 is the negative of the integral over $d\tilde{q}$, thus the integrand between curly brackets is always negative. This causes $\mathcal{M}$ to be always less than or equal to zero, with it only being zero if $q=q_0$ throughout the domain (i.e. when no disturbances, or waves, are present). Note that this result is tied to the definition of $q_0$ being monotonically increasing, because only then is the sign of $\left[Y(q_0+\tilde{q})-Y(q_0)\right]$ determined by the sign of $q-q_0$.

As remarked in [14], the general basic state $q_0$ used in Eq. 2.3.1, can also be chosen to be the zonal mean QGPV ($\bar{q}$) described by Eq. 1.3.5a. Because the zonal mean equations will then also have a vertical component, $Y(\cdot)$ will have a $z$-dependence of the form $Y(\bar{q}+q';z)$. A note here is that, by Noether's theorem, any conservation law is associated with a symmetry. In the case of $q$ in a meridional plane, the conservation of pseudomomentum still relates to the zonal symmetry of the medium (e.g. McIntyre and Shepherd [15] section 7), as it did for the barotropic example surrounding Eq. 2.3.1. In the following, the $z$-dependence of $Y$ is omitted, with the note that the integral of Eq. 2.3.3 is instead to be taken over the $(y,z)$-domain. In QG-theory, $\bar{q}$ dominates the QGPV budget. This can be used as a basis for a small amplitude assumption of the form $q' \ll \bar{q}$, where $q=\bar{q}+q'$. Using this to expand $Y(\bar{q}+q')$ to second-order, gives

$$Y(\bar{q}+\tilde{q}) \approx Y(\bar{q}) + \tilde{q}\left.\frac{\partial Y}{\partial q}\right|_{\bar{q}} + \mathcal{O}(3). \tag{2.3.2}$$

Inserting this in Eq. 2.3.1 and evaluating the integral over $d\tilde{q}$ from 0 to $q-\bar{q}=q'$, gives the integrand between curly brackets as

$$-\frac{{q'}^2}{2\partial_y \bar{q}}, \tag{2.3.3}$$

where it was used that $\partial_q Y\big|_{\bar{q}} = \partial_{\bar{q}} y \approx (\partial_y \bar{q})^{-1}$ by the definition of $Y$. Note that $\partial_y \bar{q}$ is positive because of the background planetary vorticity gradient, and hence Eq. 2.3.3 is negative definite. Because the integrand of Eq. 2.3.1 is integrated over the entire domain to find $\mathcal{M}$, the integrand itself represents a 'density' of pseudomomentum. As such, Eq. 2.3.3 represents the second-order pseudomomentum density per unit mass of small-amplitude quasi-geostrophic planetary waves. Much of the importance of Eq. 2.3.3 lies in the notion that it will appear in a wave conservation law in Ch. 3, namely Eq. 3.1.4. There the time development of Eq. 2.3.3 will be shown to relate to meridional eddy fluxes of $q$. This will formalize the relation between the sign of $\overline{v'q'}$ and the development of planetary waves, as discussed in section 2.1.

As is discussed in Appendix A.2, when waves interact with their medium, it is often 'as if' the waves have momentum equal to their pseudomomentum. Such an analogy also hold for planetary waves, as will follow from the discussion in section 1.3. There it will be shown that the sign of planetary wave zonal pseudomomentum growth is equal to the sign of the zonal forcing, which comes in the form of EP-vector divergence. The importance of planetary wave pseudomomentum being negative definite, lies in the notion that the waves can then only transport negative momentum away from their source region. Or conversely, that they can only transport zonal momentum towards their source region and away from the region where they propagate to (or 'break', as will be discussed in section 2.4). This accelerates the zonal flow in regions where they propagate away from, and decelerates the zonal flow in the regions where

the propagate to. By this mechanism, vertically propagating planetary waves drive the surface westerlies and the poleward stratospheric Brewer-Dobson circulation.

## 2.4 Planetary wave breaking and critical layers

The effects of a planetary wave entering a layer of fluid were discussed in terms of a PV-budget in section 2.1. It was argued that in the context of a quasi-geostrophic shallow water $\beta$-plane, undulations of a PV-contour bring about meridional eddy fluxes of $q$, which are equivalent to a negative zonal forcing through Eq. 2.1.4. If a planetary wave would enter and subsequently leave the layer, the eddy fluxes of $\overline{v'q'}$ cancel each other out, and the net effect on the mean flow would be zero. The initially straight PV-contour will have been deformed, and then restored back again to its original shape. This can only happen if the initial deformation is a reversible process. If the deformation of the PV-contour is irreversible, the undulation of the contour becomes permanent, and corollary the negative zonal forcing associated with $\overline{v'q'} < 0$ also becomes permanent. This irreversible deformation is defined as planetary wave breaking, which will be discussed in this section.

Breaking of planetary waves frequently occurs in the mid-latitude stratosphere, which is referred to as the 'stratospheric surf-zone' (a term coined by McIntyre and Palmer [16]). This choice of word rests on the analogy between the surf-zone of a typical beach, where ocean gravity waves grow in amplitude and break. The stratospheric surf-zone, henceforth referred to simply as the surf-zone, is a 'nonlinear critical layer'. A critical layer is defined as a zone in which nonlinear wave-dynamics become important, relative to their linear dynamics. For reference, comprehensive (analytical) discussions on the interaction between linear and non-linear dynamics surrounding planetary wave critical layers, can be found in, for example, North *et al.* [14] pp. 317-332, and Bhler [17] Ch. 7.

During wintertime, the zonal winds associated with the stratospheric polar vortex are latitudinally sheared. This ties in with the general structure of the polar night jet, as can be observed in the top right panel of Fig. A.9 in Appendix A.8. The latitudinal shear of the zonal wind implies that the winds decrease southwards of the jet core. In section 2.2, it was mentioned that planetary waves tend to grow in amplitude and bend equatorwards as they propagate upwards. As they propagate vertically, planetary waves will therefore come into contact with regions where the zonal winds become weaker. In [14] pp. 317-318, the interaction between the shear flow and equatorwards moving planetary waves is discussed in the idealized context of a shallow water $\beta$-plane. For linear planetary waves with zonal phase speed $c$, imposed on a linear positive South-to-North shear flow $U(y)$, the stability of the shear flow is found to break down at the critical line where $U(y_c) = c$. At the critical line, the solution of the waves' zonal phase speed $c$ becomes unphysical, due to a singularity in the linear equations (following the discussion surrounding Eq. 3, p. 318 from [14]). For $y > y_c$ the solutions are that of normal planetary waves, and for $y < y_c$ the waves are found to be evanescent. To resolve the singularity at the critical line, nonlinear terms (right-hand side of Eq. 2, p. 318 from [14]) must be resolved in the region surrounding the critical line. In this region, called the critical layer, the PV-contours tend to wrap up in a typical Kelvin cat's eye structure. This structure, together with the aforementioned properties of the wave solution, are sketched in Fig. 2.4 for stationary planetary waves ($c = 0$ such that $y_c = 0$).

As vertically propagation planetary waves bend equatorwards and grow in amplitude on a meridionally sheared zonal flow, their linear description will at some fail, and their PV-contours will become wrapped up in a nonlinear critical layer. With this wrapping action, the contours

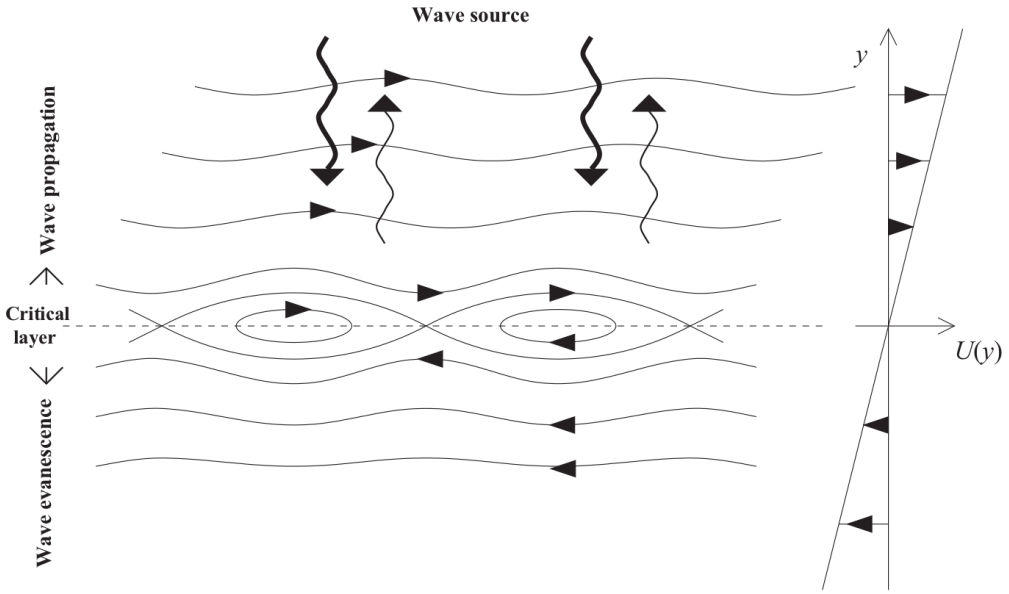


**Figure 2.4:** Illustration of a planetary wave critical layer for stationary planetary waves on a latitudinally sheared zonal flow. Arrows on the streamlines indicate direction of the flow. Arrows oriented in the $y$-direction represent meridional displacement of zonally propagating planetary waves. Figure retrieved from North *et al.* [14], p. 319.

come to lie closer and closer to each other. As the wrapping progresses to smaller scales still, it becomes irreversible and the PV in the critical layer becomes mixed. The associated Kelvin cat's eye pattern stems from an analytical solution of a nonlinear critical layer, which in literature is referred to as the Stewartson-Warn-Warn solution (e.g. Haynes and McIntyre [18] for a description). The Kelvin cat's eye pattern of planetary wave breaking occurs frequently in the real atmosphere, as can be seen from the observations in Appendix A.8, Fig. A.7, Fig. A.9 and Fig. 1.2.

The meridional displacement of planetary waves, is itself influenced by the critical layer. The critical layer is said to either, (1) absorb, then only waves 'bending' equatorwards exist, (2) reflect, then polewards deflected waves also exist, (3) over-reflect, the critical layer emits planetary waves, such that there are more poleward than equatorwards propagating waves. The dynamics of these three 'configurations' of the critical layer, are considered in detail in Killworth and McIntyre [19]. The equatorward and poleward moving waves are also drawn in Fig. 2.4, represented by the meridional arrows. The exact behavior of the critical layer depends on the characteristics of the flow inside of it. However, an intuitive example is given by a critical layer in which the PV-gradient has been reduced to zero by breaking planetary waves. This is referred to as a 'mature' critical layer. Because planetary waves can only exist on a PV-gradient (section 2.1, a mature critical layer cannot sustain planetary waves, and it will thus reflect incoming waves.

When planetary waves break, their wave character seizes to exist, and the effect that the waves would normally have on the mean flow becomes permanent. As argued in section 2.1, the introduction of a planetary wave is associated with downgradient zonal mean meridional eddy fluxes of $q$, i.e. $\overline{v'q'} < 0$. When planetary wave breaking evolves into turbulent mixing of $q$, it then 'follows' that turbulent mixing is also associated with downgradient eddy fluxes $q$. This notion is indeed in line with the theory of geostrophic turbulence, from which a result is that diffusive quasi-geostrophic turbulence, associated with $q$ cascading to smaller scales and

corollary planetary wave breaking, transports and mixes $q$ systematically downgradient (e.g. Rhines [20] and Held [21]).

# Chapter 3

# Wave-mean flow interaction

In this chapter, planetary wave-mean flow interaction, the surf-zone and planetary waves on a sharp PV-gradient, will be treated in terms of a quasi-geostrophic PV budget. In doing so, many of the concepts described in Ch. 2 will be brought together in a unifying PV-view of the dynamics. Core theoretical concepts are the Taylor-identity, linking the divergence of wave-induced momentum fluxes to eddy fluxes of (QG)PV, and a wave-conservation law for planetary waves. Furthermore, a selection of results from quasi-geostrophic theory will be tested and expanded upon using numerical piecewise PV-inversion experiments of Rossby-Ertel PV. In particular, the angular momentum changes associated with up and downgradient eddy fluxes of PV will be considered.

## 3.1 Eliassen-Palm diagnostics

An important result in zonal mean quasi-geostrophic theory, is the so-called Taylor-identity. This identity links (zonal mean) meridional eddy fluxes of $q$ to the divergence of the Eliassen-Palm (EP) vector. Divergence of the EP-vector also represents an 'implicit' zonal force, which is expressed through the PV-inversion principle. Furthermore, EP-vector divergence is coupled to the growth of planetary wave pseudomomentum, discussed in section 2.3, through a wave-conservation law. The goal of this section is to use the wave-conservation law to describe the effect of planetary wave propagation and dissipation on the mean flow.

The Taylor-identity follows from the multiplication of $q'$, defined by Eq. 1.3.5a and the separation $q = \bar{q} + q'$, with the meridional geostrophic velocity perturbation $v'$ (Appendix 3.1). The derivation requires only the splitting of variables in a mean and eddy term, and the identity is therefore generally valid, meaning that no small-amplitude assumption is needed. With $\nabla = (\partial_y, \partial_z)$, the Taylor-identity is written as

$$\overline{v'q'} = -\frac{\partial}{\partial y}\overline{u'v'} + \frac{\partial}{\partial z}\left(\frac{f_0}{N^2}\overline{v'b'}\right) = \nabla \cdot (F^{(y)}, F^{(z)}), \tag{3.1.1}$$

where $F^{(y)}$ and $F^{(z)}$ are the meridional and vertical components of the Eliassen-Palm (EP) vector $F$, respectively. Writing Eq. 3.1.1 in terms of EP-vector divergence is a matter of convention, which was embraced shortly after the vector appeared in Transformed Eulerian Mean (TEM) theory, first published in a paper by Andrews and McIntyre [22]. A key result of TEM-theory, is that it interprets EP-vector divergence as a single eddy forcing term appearing in the zonal momentum budget (TEM-equivalent of Eq. 1.3.4a). Namely, that a converging EP-vector ($\overline{v'q'} < 0$) and diverging EP-vector ($\overline{v'q'} > 0$) are a negative and positive 'transformed' zonal

momentum forcing, respectively. In TEM-theory, having a single eddy term in the governing equations is an 'improvement' over the conventional equations given by Eq. 1.3.4a - Eq. 1.3.4d, which contain the two separate eddy forcing terms proportional to $\overline{v'b'}$ and $\overline{u'v'}$, respectively. In the conventional Eulerian mean, the eddy terms force a system which is coupled by the free variables $\bar{u}$, $\bar{v}_a$, $\bar{w}_a$ and $\bar{b}$. However, because of thermal wind balance (Eq. 1.3.4c), the effect of the eddy momentum and eddy buoyancy forcings cannot be clearly separated. The appeal of TEM-theory, is that this ambiguity in the eddy forcing is removed. However, TEM-theory requires an alternative definition of the zonal mean ageostrophic circulation. This complicates its physical interpretation, especially when it is compared to observations from a conventional Eulerian mean picture of the atmosphere. In this chapter, the Taylor-identity will be interpreted solely in terms of the meridional eddy flux of $q$, avoiding TEM-theory altogether.

In Eq. 3.1.1, the divergence of the eddy momentum term $\overline{u'v'}$ relates to a zonal force by virtue of its appearance in Eq. 1.3.4a. As was mentioned in section 2.2, the divergence of the eddy buoyancy term in Eq. 3.1.1 also relates to a zonal force. This is through the mechanism of 'form drag', and it relates to the force exerted by wave-induced deformation of pressure surfaces in a stratified fluid (Appendix A.4). With EP-vector divergence being the sum of two zonal force terms, divergence of the EP-vector itself also relates zonal force. The complication of this, lies in the notion that the EP-vector does not by itself appear in the zonal momentum budget of Eq. 1.3.4a. The zonal forcing is instead 'implicitly' governed by the eddy term $\overline{v'q'}$. By the PV-inversion principle, $q$ relates to the momentum field through a balanced assumption. That way, changes in the distribution of $q$, relate to changes in the angular momentum distribution. The significance of Eq. 3.1.1, then lies in the observation that in zonal mean QG-theory, the distribution of $q$ can only be altered by fluxes of $\overline{v'q'}$ (Eq. 1.3.6). How exactly a redistribution of $q$ affects the angular momentum budget, will be considered in an example in section 3.2. There, conserved downgradient transport of $q$, equivalent to a converging EP-vector, will be directly associated with angular momentum loss (i.e. a retrograde, westward force).

The interpretation of EP-vector divergence reaches beyond that of a zonal forcing. This was already hinted at by the discussion in section 2.1, where the introduction of a planetary wave was associated with negative eddy fluxes of $q$. Indeed, as discussed in Edmon Jr *et al.* [23] sections *b* and *d*, the EP-vector can also be used to study the growth, propagation and dissipation of planetary waves. This is motivated by the appearance of EP-vector divergence in a wave-conservation law, which will now be derived. The first step is to linearize the equation for the time-development of $q$, given by Eq. 1.3.5b, around a perturbation $q'$. Expanding the terms in a mean and perturbation part with the assumption that $q' \ll \bar{q}$, and zonally averaging, yields

$$\frac{\partial \bar{q}'}{\partial t} + \overline{v' \frac{\partial \bar{q}}{\partial y}} = \overline{\chi'}. \tag{3.1.2}$$

Multiplying Eq. 3.1.2 by $q'$, dividing by $\partial_y \bar{q}$ and writing $q' \partial_t q' = \partial_t (q')^2/2$, gives

$$\left(\frac{\partial \bar{q}}{\partial y}\right)^{-1} \frac{\partial (\bar{q'})^2}{2\partial t} + \overline{v'q'} = \left(\frac{\partial \bar{q}}{\partial y}\right)^{-1} \overline{q'\chi'}. \tag{3.1.3}$$

Using the assumption that $\partial_y \bar{q}$ is independent of $t$, Eq. 3.1.3 can be written as

$$\frac{\partial A}{\partial t} + \nabla \cdot F = D, \tag{3.1.4}$$

where the wave-activity $A = \overline{(q')^2/2\partial_y \bar{q}}$ is defined as the negative of the planetary wave pseu-

domomentum density (Eq. 2.3.3), and the sources and sinks of non-conservative wave effects[1] is defined as $D = \overline{q'\chi'/\partial_y \bar{q}}$. Eq. 3.1.4 is a conservation law for small-amplitude planetary waves, referred to as the 'Eliassen-Palm relation' (e.g. Vallis [2] section 10.2.1). For steady small-amplitude waves ($\partial_t A = 0$) in adiabatic and frictionless conditions ($D = 0$), it follows from Eq. 3.1.4 that $\nabla \cdot F = 0$. A non-divergent EP-vector in turn corresponds to $\overline{v'q'} = 0$, which by Eq. 1.3.6 implies that the zonal mean time development of $q$ is also zero ($\partial_t \bar{q} = 0$). This in turn relates to the time development of the full flow, as is dictated by PV-inversion. With the assumption that the presence of eddies does not affect the boundary conditions for PV-inversion, $\partial_t \bar{q} = 0$ implies that the flow is steady. In terms of the full equations of motion, a steady flow implies that in Eq. 1.3.4a and Eq. 1.3.4d, $\partial_t \bar{u}$ and $\partial_t \bar{b}$ are zero. Eddies are however still present, namely in the form of steady small-amplitude planetary waves. A non-divergent EP-flux then implies that the eddy terms in 1.3.4a and Eq. 1.3.4d, are exactly balanced by the ageostrophic circulation, such that $\partial_t \bar{u} = \partial_t \bar{b} = 0$. This is known as the non-acceleration theorem for steady small-amplitude planetary waves, where 'non-acceleration' refers to the mean flow being unaffected by the eddies.

The orientation of the EP-vector in the meridional plane, holds information on where planetary waves are propagating to. By its definition, the orientation of the EP-vector represents the magnitude of the eddy momentum and eddy buoyancy terms. However, for conservative flows ($\chi = 0$, and corollary $D = 0$), Eq. 3.1.4 takes on the form $\partial_t A + \nabla \cdot F = 0$. Wherever $F$ converges, $A$ increases, and wherever $F$ diverges, $A$ decreases. This makes $F$ a measure of where planetary wave activity is propagating to. By this mechanism, Eq. 3.1.4 describes the interaction between the momentum of the mean flow and the pseudomomentum of planetary waves. The notion of $F$ being a measure of where planetary waves are propagating to, can be made explicit when the waves are assumed to be governed by linear planetary wave theory, including the assumption that the medium varies slowly in time (e.g. Vallis [2] section 10.2.2). With these assumptions, the EP-vector can be written as $F = (c_g^y A, c_g^z A)$, where $c_g^y$ and $c_g^z$ are the meridional and vertical component of the planetary wave group velocity vector $\mathbf{c}_g$, respectively. With $F$ parallel to the group velocity of the waves, its orientation in the meridional plane gives a sense of where planetary waves are propagating to following their group velocity.

Eliassen-Palm cross sections of the troposphere and lower stratosphere are a frequently used diagnostic tool for planetary waves and their mean flow interaction. In the meridional plane, the orientation of $F$ indicates the direction in which planetary waves are propagating. The convergence of $F$ ($\overline{v'q'} < 0$) shows where planetary waves dissipate, or break, and lead to angular momentum loss (section 3.2). Regions in which $F$ diverges ($\overline{v'q'} > 0$), show where planetary waves propagate away from their source region and accelerate the mean flow. Generally speaking, $\chi$ (Eq. 1.3.4a) and corollary $D$ (Eq. 3.1.4) are non-zero in planetary wave source regions. Put differently, $\chi$ and $D$ are non-zero in regions where wave-activity ($A$) is generated. This complicates the description of planetary wave source regions in terms of a 'PV-view', as PV is not conserved when $\chi$ is non-zero. A more detailed description of planetary wave dynamics with respect to their source region, falls outside the scope of this thesis. The idea is that once wave-activity is generated in a source region, planetary waves accelerate the mean flow by propagating away from this source region. This notion is in line with the waves' pseudomomentum being negative definite, as is discussed in section 2.3.

[1] In regions where quasi-geostrophic theory is a good approximation, $D < 0$ is associated with wave dissipation by Rayleigh friction and Newtonian cooling and $\partial_t A > 0$ with growing waves (Andrews [24], section 2).

## 3.2 The surf-zone and angular momentum loss

In section 1.3, it was discussed that the zonal forcing of EP-vector convergence is 'implicit', in the sense that a redistribution of QGPV relates to the angular momentum budget only through PV-inversion. In previous sections it was also discussed that the zonal mean QGPV ($q$) can exclusively be transported by the term $\overline{v'q'}$, and that planetary wave breaking is associated with downgradient mixing of $q$ ($\overline{v'q'} < 0$). In this section, the effects of such downgradient transport on the zonal momentum budget will be demonstrated using an idealized 'mixing-zone'. This mixing-zone is represented by a region in which downgradient transport of $q$ by planetary wave breaking, has reduced the QGPV-gradient to zero.

The following example[2] takes place in the context of an unbounded shallow water quasi-geostrophic $\beta$-plane. In shallow water QG-theory, the zonal angular momentum invariant relates to the zonal symmetry of the medium. This abstract notion is tied to the same type of analysis used to derive the zonal pseudomomentum in section 2.3 (e.g. North *et al.* North *et al.*, pp. 324 - 331). The expression for the absolute zonal angular momentum per unit horizontal area ($M$) in a shallow water $\beta$-channel, is given by $M = \rho_0 H(y)\left[u(y) - fy\right]$, which is the one-dimensional unit mass version of Eq. 29 from North *et al.* p. 328. Here $f$ is the Coriolis parameter as in Eq. 1.3.3, $H(y)$ is the local layer depth, $u(y)$ is the local zonal velocity and $y$ is the meridional coordinate on a $\beta$-plane. The layer depth $H(y)$ can be written as $H(y) = H_0 + h(y)$, where $H_0$ is scaled as $H_0 = f_0^2 L_d^2 g^{-1}$. Here $L_d$ is the Rossby radius of deformation defined as $L_d = \sqrt{gH_0}/f_0$, and $g$ the acceleration due to gravity. The expression for $M$ can then be written as

$$M = \rho_0 \left[H_0 + h(y)\right]\left[u(y) - f_0 y\right], \tag{3.2.1}$$

where the flow (i.e. the region in which $\delta M$ is non-zero) is constrained to a region where $f \approx f_0$. If $h(y)$ and $u(y)$ are chosen to be perturbation terms $\delta u(y)$ and $\delta h(y)$ of an initially motionless state ($h(y) = u(y) = 0$), the quasi-geostrophic expression for $\delta M$, using Eq. 3.2.1, becomes $\delta M = \rho_0 H_0 \delta u(y) - \rho_0 f_0 y \delta h(y)$. Note that in QG-theory, terms involving products of perturbations are ignored. In the context of total angular momentum change, $\delta M$ over the entire domain is the quantity of interest. In integral form, this is written as

$$\delta M = \rho_0 \int_{-\infty}^{\infty} [H_0 \delta u(y) - f_0 y \delta h(y)] dy, \tag{3.2.2}$$

where it was used that $\delta u(y) = -\partial_y \delta\psi$ and $\delta h(y) = f_0 \delta\psi g^{-1}$ by the definition of the stream-function $\psi$, defined in section 1.3. The next step is to write $\delta M$ in terms of a perturbation of shallow water QGPV ($\delta q$). The expression for shallow water QGPV is (e.g. Vallis [2] Eq. 5.9),

$$q = \beta y + \nabla^2 \psi - L_d^{-2} \psi. \tag{3.2.3}$$

The first order (geostrophic) perturbation of Eq. 3.2.3, is $\delta q = \partial_y^2 \delta\psi - L_d^{-2}\delta\psi$. Note that for a zonal mean flow, $\nabla^2 = \partial_y^2$. Using the definition of $h(y)$ and $H_0$, $\delta h(y)$ can also be written as $\delta h(y) = f_0^{-1} H_0 L_d^{-2} \delta\psi$. Inserting this, as well as the definition of $\delta u(y)$ in terms of $\psi$, in Eq. 3.2.2, yields

$$\begin{aligned}
\delta M &= \rho_0 H_0 \int_{-\infty}^{\infty} [-\partial_y \delta\psi - L_d^{-2} y \delta\psi] dy \\
&= \rho_0 H_0 \int_{-\infty}^{\infty} y[\partial_y^2 \delta\psi - L_d^{-2}\delta\psi] dy \\
&= \rho_0 H_0 \int_{-\infty}^{\infty} y \delta q(y) dy.
\end{aligned} \tag{3.2.4}$$

[2] This is an adaptation of the example from section 7 in Dritschel and McIntyre [9].

In the second to last step, it was used that $\partial_y(y\partial_y\delta\psi) = \partial_y\delta\psi + y\partial_y^2\delta\psi$. Integrating the left-hand side of this expression with respect to $y$ amounts to zero, because the induced velocity field $u(y) = -\partial_y\psi$ (and corollary $\delta u$) is 0 infinitely far away from the PV-anomaly, and hence $-\int \partial_y\delta\psi = \int y\partial_y^2\delta\psi$.

Eq. 3.2.4 links a change in absolute zonal momentum to a change in the QGPV-distribution. This relation works both ways, such that for a given $\delta q(y)$, Eq. 3.2.4 can be used to calculate $\delta M$. For example, consider a QGPV-distribution representing a mixing-zone as in panel (a) of Fig. 3.1. This figure represents a region in which downgradient mixing of $q$ by planetary wave breaking, has completely homogenized the QGPV-gradient in the mixing-zone. The resulting anomaly $\delta q(y)$ is N-shaped, as in panel (b) of Fig. 3.1. For this mixing-zone configuration, $\int \delta q(y)dy = 0$, highlighting the notion that $q$ is conserved over the course of a planetary wave breaking event. The mixing-zone is centered over $y_0 = 0$, and is bounded by $|y| \leq b$. The dotted

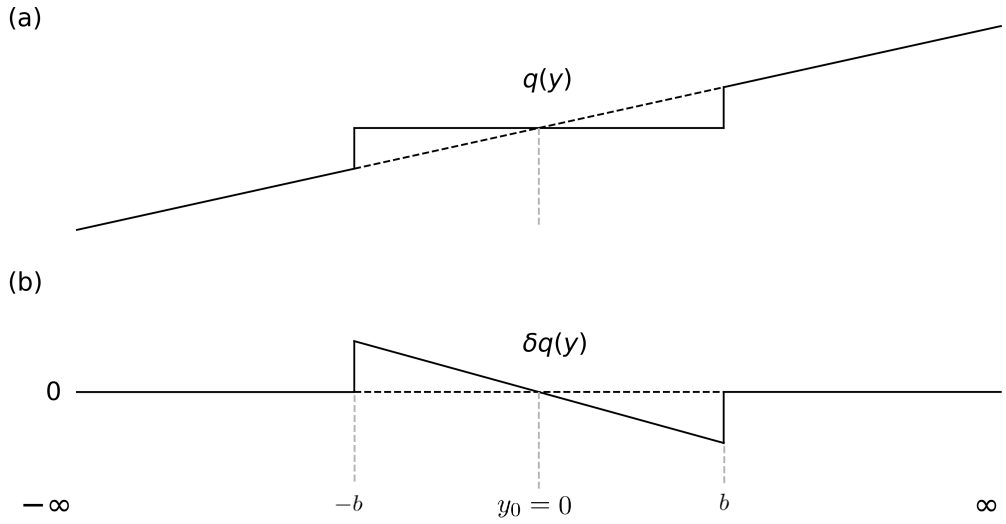


**Figure 3.1:** Panel (a): shallow water QGPV gradient $q(y)$ on an infinitely large $\beta$-plane, with a completely mixed surf-zone centered around $y_0$. Panel (b): local deviation $\delta q(y)$ from the background potential vorticity gradient.

grey line in panel (a) of Fig. 3.1, corresponds to a motionless atmosphere where $\partial_y f = \beta$, with $f$ as in Eq. 1.3.3. By inspection of panel (b), the relation between $\beta$ and $\delta q(y)$ is given by $\delta q(y) = -y\tan(\beta)$ for $|y| \leq b$, and $\delta q(y) = 0$ otherwise. Inserting this expression for $\delta q(y)$ in Eq. 3.2.4, gives

$$\begin{aligned}\delta M &= \rho_0 H_0 \int_{-b}^{b} -y^2 \tan(\beta) dy \\ &\approx -\frac{2}{3}\rho_0 H_0 \beta b^3,\end{aligned} \tag{3.2.5}$$

where the small angle approximation $\tan(\beta) \approx \beta$ was used. Eq. 3.2.5 represents the net momentum change due to QGPV-mixing in the highly idealized mixing-zone of Fig. 3.1. All the factors in Eq. 3.2.5 are positive, and hence $\delta M$ is negative. This signifies that the angular momentum change is negative when conserved QGPV is mixed down-gradient. The association between downgradient mixing of QGPV and angular momentum loss, generalizes to more sophisticated 'staircase' configurations (with Fig. 3.1 representing a single step), as is discussed in Wood and McIntyre [25]. In section 5 and appendix A of [25], two separate proofs are given for the sign of $\delta M$ being negative for any downgradient re-configurations of stratified (or multi-layered)

QGPV, provided that the background QGPV-gradient is monotonically increasing. The proofs themselves are rather technical, but nonetheless, the essence is captured by the highly idealized example of Eq. 3.2.5.

The idealized mixing-zone in Fig. 3.1, represents the PV-configuration that occurs after breaking planetary waves mix $q$ downgradient through negative eddy fluxes of $\overline{v'q'}$. The corresponding downgradient mixing of $q$, causes sharp vorticity gradients to form along the edges of the mixing-zone, as can be seen in panel (a) of Fig. 3.1. The stratospheric surf-zone, where planetary wave breaking is commonplace, is then effectively a large mixing-zone. In reality however, the sharp equatorward gradient of Fig. 3.1 is less pronounced than the poleward gradient, as can be seen in Appendix A.8 Fig. A.11. This is because the PV-gradient is not shaped only by downgradient mixing by planetary wave breaking, but also by diabatic processes. The dominant PV-gradient which is associated with the edge of the polar vortex, is however still 'sharpened' by planetary wave breaking. This sharpening process plays an important role in the dynamics that help to maintain the polar night jet and surf-zone structure, as will be discussed in section 3.3.

On the timescale of planetary wave breaking events, conditions in the stratosphere are approximately adiabatic and frictionless. This implies that $\chi = 0$ in Eq. 1.3.5a, and corollary $D = 0$ in the wave-conservation law given by Eq. 3.1.4. The wave-conservation law then reduces to $\partial_t A + \nabla \cdot F = 0$, where $\nabla \cdot F = \overline{v'q'}$ as in Eq. 3.1.1. Using the wave-conservation law, negative eddy fluxes of $\overline{v'q'}$ correspond to an increase in planetary wave-activity ($\partial_t A > 0$). But as discussed in section 2.4, $\overline{v'q'} < 0$ also relates to planetary wave breaking. The difference between the two interpretations of $\overline{v'q'}$ lies in the fact that the wave-conservation law assumes small-amplitude linear waves, whereas wave breaking is associated with irreversible non-linear effects, where waves lose their wavelike characteristics. This makes planetary wave breaking a sink of planetary wave-activity. For this reason, planetary wave activity is said to converge into the surf-zone (e.g. North *et al.* [14], p. 382).

## 3.3 Sharp PV-gradients and self-sharpening jets

By comparing Fig. A.11 and the top right panel of Fig. A.9 in Appendix A.8, it can be seen that the location of the strong PV-gradient associated with the edge of the polar vortex, corresponds to the location of the strongest zonal winds. This ties in with the notion that sharp PV-gradients induce jet structures, or localized strong currents. This notion will be examined in this section using the simplest example of a sharp PV-gradient, namely that of a shallow water quasi-geostrophic 'PV-step'. Part of the motivation of this section, lies in the observation that in Fig. 3.1 in section 3.2, downgradient mixing of QGPV is associated with the formation of sharp QGPV-gradients along the edges of the mixing-zone. This implies that, even though downgradient mixing of QGPV by planetary wave breaking leads to angular momentum loss, the jet(s) on the flanks of the mixing-zone accelerate. The mixing itself is facilitated by planetary wave breaking, which ties in with the existence of critical layers, as discussed in section 2.4. The inherent existence of critical lines for planetary waves on a sharp PV-gradient, will also be discussed in this section.

A sharp zonal mean shallow water QGPV-gradient is constructed as follows, (1) the large-scale flow is assumed to be adiabatic and frictionless, such that $q$ is conserved, (2) the QGPV-distribution is assumed to be piecewise uniform, with two uniform regions being separated by a step of height $\Delta q$, (3) the jet is assumed to be narrow such that $f \approx f_0$, fixing the Rossby radius of deformation ($L_d$). Under these conditions, the zonal mean QGPV-distribution centered

around $y = 0$ can be written as

$$Q(y) = f_0 + \frac{\Delta q}{2}\text{sgn}(y), \tag{3.3.1}$$

where sgn$(y)$ returns the sign of $y$. The expression for the zonal mean shallow water QGPV (Eq. 3.2.3) can be written as $q(y) = f_0 + \partial_y^2\psi - L_d^2\psi$. Setting $q(y)$ to be the QGPV-distribution represented by $Q(y)$, results in

$$\frac{\Delta q}{2}\text{sgn}(y) = \frac{\partial^2\psi}{\partial y^2} - \frac{\psi}{L_d^2}, \tag{3.3.2}$$

which is an inhomogeneous Helmholtz equation. $\psi$ can be solved separately for $y < 0$ and $y > 0$, using the boundary condition that the induced velocity field is zero at $\pm\infty$. Glueing the solutions together at $y = 0$, then yield a single expression. The zonal wind profile $(-\partial_y\psi)$ which arises is (e.g. Harvey *et al.* [26] Eq. 2.4),

$$U(y) = \frac{\Delta q}{2}L_d e^{-|y|/L_d}. \tag{3.3.3}$$

The character of the solution of $U(y)$, is such that the strength of the zonal jet is proportional to magnitude of the PV-step and the Rossby radius of deformation $L_d$, with the latter also affecting the meridional extent of the jet. For constant $L_d$, it can then be understood that an increase of the QGPV-gradient along the edge of a mixing-zone, attributed to downgradient QGPV-mixing by breaking planetary waves, leads to an acceleration of the jet(s) adjacent to the mixing zone. The peculiarity of this, lies in the notion that downgradient mixing by breaking planetary waves leads to net angular momentum loss, as is discussed in section 3.2, whereas the jet(s) along the edges of the mixing-zone accelerate[3].

A sharp PV-front also by itself supports planetary waves[4]. Following the discussion in [26], the position of material PV-contours in a horizontal plane, is represented by the function $\eta(x, y, t)$. A kinematic argument links the total time derivative of $\eta$ to advection of the contour by the meridional wind $v$, through

$$\left(\frac{\partial}{\partial t} + u\frac{\partial}{\partial x}\right)\eta(x, y, t) = v. \tag{3.3.4}$$

Undulations of the contours are assumed to be small-amplitude disturbances of the form $\eta(x, y, t)$ $= \hat{\eta}(y)\exp\left[ik(x - ct)\right]$. The function $\hat{\eta}(y)$ represents meridional meanders of the contours. Other variables are split as $q = Q(y) + q'$, $u = U(y) + u'$, $v = v'$, where the perturbation terms are small and where $Q(y)$ and $U(y)$ are as in Eq. 3.3.1 and Eq. 3.3.3, respectively. In terms of the streamfunction $\psi$, the meridional velocity perturbation can be written as $v' = \partial_y\psi'$. The streamfunction perturbation itself can be calculated by inverting an equation similar to that of Eq. 3.3.2, but with the left-hand side as $-\eta(x, 0, t)\Delta q$ sgn$(y)$. This yields (e.g. Harvey *et al.* [26] Eq. 2.7 and 2.8),

$$\psi' = \phi(y, k)\hat{\eta}(0)e^{ik(x-ct)}, \tag{3.3.5}$$

where

$$\phi(y, k) = \frac{\Delta q}{2\kappa}L_d e^{-\kappa|y|/L_d}. \tag{3.3.6}$$

The function $\phi(y, k)$ represents meridional meanders of the streamfunction, and in Eq. 3.3.6, the 'effective wavenumber' is defined as $\kappa^2 = 1 + k^2L_d^2$. Using the expressions for $\psi'$, $U(y)$ and

[3] A more comprehensive and analytical discussion of this concept, is given by 'The simplest jet-resharpening problem' in Wood and McIntyre [25] pp. 1269-1270.

[4] The shallow water QG dispersion relation for planetary waves on a sharp PV-gradient, is different from the 'regular' shallow water dispersion relation given by Eq. 2.1.2.

$Q(y)$ to linearize Eq. 3.3.4 around the QGPV-step, gives

$$(U(y) - c)\hat{\eta}(y) = \phi(y, k)\hat{\eta}(0). \tag{3.3.7}$$

The solution for the meridional meanders of the PV-contours is, using Eq. 3.3.7,

$$\hat{\eta}(y) = \hat{\eta}(0)\frac{\phi(y)}{U(y) - c}, \tag{3.3.8}$$

where the zonal phase speed ($c$) of the waves is given by the sum of the wave's phase speed and the velocity of the background zonal wind $U(y)$. The waves represented by Eq. 3.3.7 reside on the QGPV-step centered at $y = 0$, such that $c = U(0) - \phi(0, k)$. Inserting the definition of $U(y)$ and $\phi(y, k)$ in the expression for $c$, gives

$$c = \frac{\Delta q}{2} L_d \left(1 - \frac{1}{\kappa}\right). \tag{3.3.9}$$

The importance of Eq. 3.3.9 lies in the notion that for $U(y) = c$, a singularity exists in Eq. 3.3.8. Following the discussion in section 2.4, the the singularity is located on the critical line $y_c$. In the region surrounding $y_c$, the so-called critical layer, non-linear effects come into effect, facilitating planetary wave breaking. A qualitative insight given by Eq. 3.3.8, is that the existence of critical layers is inherent to jet-structures. For the PV-structure associated with jets, planetary wave elasticity is highest on the sharp PV-gradient, and lowest in the adjacent 'mixing-zone', where planetary wave breaking is favoured. In the critical layer, irreversible deformation of PV-contours leads to downgradient mixing of PV. This sharpens the PV-gradient along the mixing-zone, which in turn accelerates the jet core and increases its resilience, or planetary wave elasticity. In literature, this phenomenon is referred to as a self-sharpening jet, and it plays an important role in the jet's ability to 'efficiently' maintain its structure. A more comprehensive description of the dynamics of a self-sharpening jet, can be found in, e.g., Dritschel and Scott [27], Harvey *et al.* [26], Wood and McIntyre [25] and McIntyre [28].

## 3.4 Piecewise cyclo-geostrophic PV-inversion

The connection between a downgradient reconfiguration, or flux, of QGPV ($q$) and angular momentum loss, was generalized in a paper by Wood and McIntyre [25]. In their paper, it is mentioned that equivalent theorems for downgradient fluxes of isentropic Rossby-Ertel PV (hereafter referred to simply as PV), have not yet been found. They argue that the difficulty lies in the nonlinearity of the 'cyclostrophic' PV-inversion operator. This operator is required to perform PV-inversion on scales smaller than the large (geostrophic) scale considered by QG-theory. Cyclostrophic balance refers to the balance between the pressure gradient and centripetal force. If cyclostrophic balance is extended to also include the Coriolis force, this is referred to as 'cyclo-geostrophic' balance, or gradient wind balance. Cyclo-geostrophic is a suitable balanced assumption for both large and small scale flows, or in other words, it is a suitable assumption for flows of any Rossby number. In this section, numerical cyclo-geostrophic PV-inversion experiments are performed with idealized up and downgradient 'flux' configurations of PV. The experiments are motivated by the role of EP-vector divergence (and thus transport of QGPV by eddies) in the transfer of angular momentum between the troposphere and stratosphere. Furthermore, it can be shown that isentropic eddy fluxes of PV are approximately equal to quasi-geostrophic eddy fluxes of QGPV. This makes eddy fluxes of PV approximately equal to quasi-geostrophic EP-vector divergence, which suggests that the effects on the angular momentum budget of up

and downgradient PV transport, is similar in nature to that of QGPV-transport. The relation between isentropic eddy fluxes of PV ($\overline{v'Z'}$) and eddy fluxes of QGPV ($\overline{v'q'}$) is discussed from a theoretical and observational point of view in Appendix A.5 and A.6, respectively.

The experiments are constructed as follows, (1) numerical cyclo-geostrophic PV-inversion is performed in a meridional plane, with potential temperature as height coordinate, (2) potential temperature levels are spaced 2 Kelvin (K) apart and the meridional step size is 0.1 degrees, (3) changes in the PV-distribution are superimposed on a reference PV-distribution corresponding to a motionless atmosphere, (4) conditions are assumed to be adiabatic and frictionless, such that total PV is conserved in any redistribution of PV, (5) idealized up and downgradient configurations are constructed in a manner analogous to the mixing-zone shown in Fig. 3.1 of section 3.2. The cyclo-geostrophic PV-inversion is performed with the method described in Van Delden and Hinssen [29]. A notable assumption used is that the edges of the domain are sufficiently far away from the induced velocity field for the boundary condition $u = 0$ to be valid.

The downgradient configuration shown in the left panel of Fig. 3.2, is analogous to the 'mixing-zone' shown in panel (a) of Fig. 3.1. The upgradient configuration in the right panel of Fig. 3.2 is constructed in a manner analogous to the opposite of $\delta q$, where $\delta q$ represents a downgradient redistribution of QGPV as in panel (b) of Fig. 3.1. From a quasi-geostrophic zonal

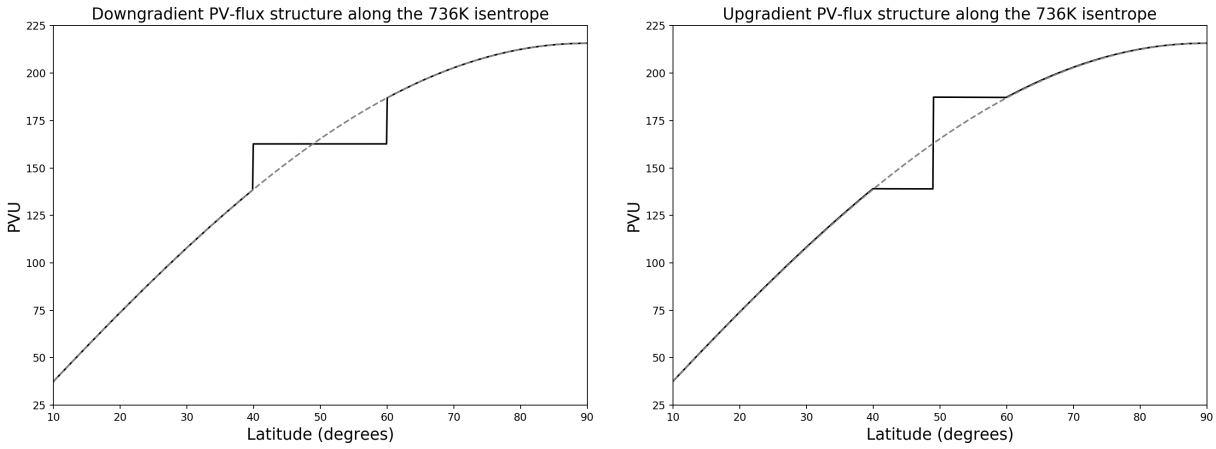


**Figure 3.2:** Idealized up and downgradient transport of cyclo-geostrophic PV along the 736K isentrope. Dotted grey line represents the reference PV-distribution, which corresponds to a motionless atmosphere. Left panel: Conserved downgradient transport between 40 and 60 degrees North. Right panel: Conserved upgradient transport between 40 and 60 degrees North. 1 PVU = $10^{-6}$ K m$^2$ kg$^{-1}$ s$^{-1}$.

mean perspective, the opposite of $\delta q$ would imply that QGPV is transported up its gradient through positive fluxes of $\overline{v'q'}$. The region where up and downgradient configurations of PV are imposed, is centered along the 736K isentrope and 50 degrees North. 736K corresponds to the middle of the domain in terms of its vertical extent, and likewise, 50 degrees North corresponds to the middle of the domain in terms of its latitudinal extent. The dotted grey lines in Fig. 3.2 represent the reference PV-distribution, corresponding to a motionless atmosphere. As discussed in Hinssen *et al.* [30], it is the deviation from this reference distribution which induces a zonal wind.

To demonstrate the character of cyclo-geostrophic PV-inversion, seven-layer thick up and downgradient configurations are inverted. Here seven-layer thick configurations are chosen over single-layer ones, because then the inverted fields are more pronounced. They are however qualitatively the same. Centered around 736K, the PV-anomalies are then vertically bounded by the 730K and 742K isentrope. The resulting zonal velocity profiles for the down and upgradient

configurations, are shown in the left and right panel of Fig. 3.3, respectively. By comparing the

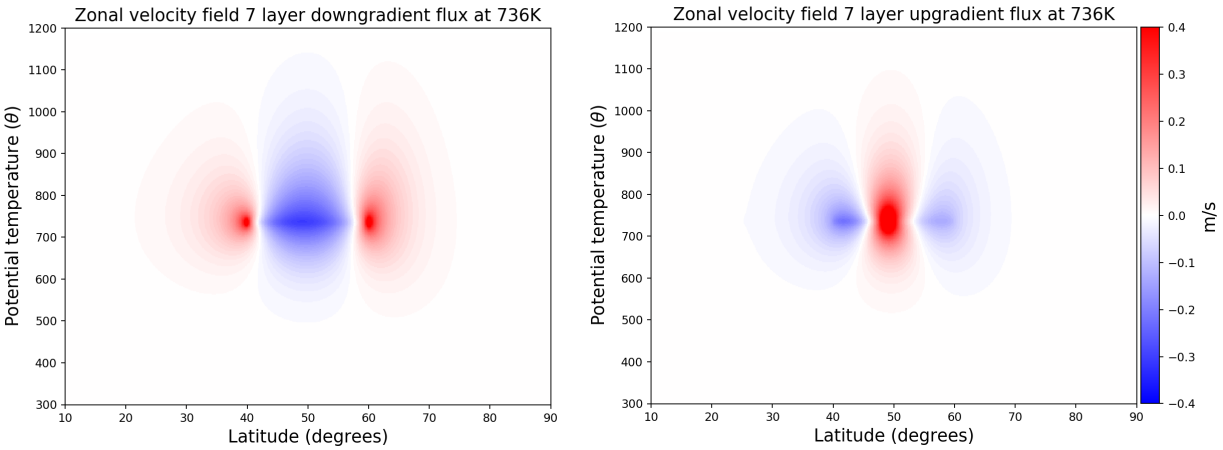


**Figure 3.3:** Induced zonal velocity fields by seven-layer up and downgradient transport of PV centered around 736K, as determined by cyclo-geostrophic PV-inversion. Left panel: Downgradient transport with each layer being as in the left panel of Fig. 3.2. Right panel: Upgradient transport with each layer being as in the right panel of Fig. 3.2.

left panel of Fig. 3.3 and Fig. 3.2, it can be seen that the sharp gradients along the edge of the 'mixing-zone', induce eastward zonal jets. This is in accordance with the quasi-geostrophic relation between sharp PV-gradients and jet structures, as discussed in section 3.3. The eastward jets along the edge of the mixing-zone and westward jet on the interior of the mixing-zone, are both in qualitative agreement with the zonal velocity field induced by a shallow water quasi-geostrophic mixing-zone (e.g. Dritschel and McIntyre [9] Fig. 7 panel 2). The same qualitative picture holds for the wind field induced by the upgradient PV-configuration. The eastward jet in the right panel of Fig. 3.3 coincides with the sharp PV-gradient shown in the right panel of Fig. 3.2, and the interior of the adjacent homogenized zones induce westward winds.

To quantify how up and downgradient configurations of PV affect the angular momentum budget, the absolute angular momentum per unit mass ($\hat{M}$) is considered. This quantity takes into account changes in angular momentum attributed to the angular momentum of the induced velocity field, as well as angular momentum changes due to a mass shift. With the assumption $r \approx a$, where $a$ is the radius of the Earth and $r$ is the distance from the Earth's center, the absolute angular momentum per unit mass is defined as (Holton and Hakim [31] p. 331)

$$\hat{M} = (\Omega a \cos\phi + u)\, a \cos\phi, \tag{3.4.1}$$

where the hat signifies the distinction between $M$ defined by Eq. 3.2.1. Using $\hat{M}$, the total angular momentum can be calculated for the reference atmosphere and for the state of the atmosphere given by PV-inversion of the configurations shown in Fig. 3.2, over the entire domain. The resulting change in absolute angular momentum per unit mass ($\delta\hat{M}$) is indicative of the effect of PV-transport on the total angular momentum budget. For a single layer downgradient configuration as in the left panel of Fig. 3.2, $\delta\hat{M}$ is plotted in the left panel of Fig. 3.4 as a function of the isentropic level on which the downgradient configuration is imposed. Note that single layer configurations are chosen in order to match the theoretical example given in section 3.2. From Fig. 3.4, it can be seen that downgradient transport of PV leads to a net reduction of angular momentum. This is in line with the result from quasi-geostrophic theory, where downgradient transport of QGPV is associated with angular momentum loss. From Fig.

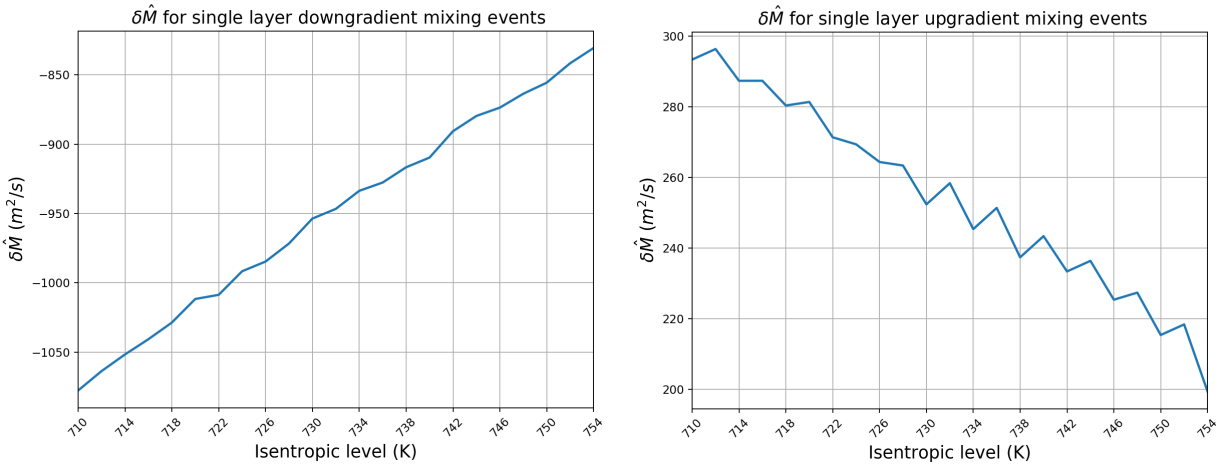


**Figure 3.4:** Change in absolute angular momentum per unit mass ($\delta\hat{M}$), as determined by cyclo-geostrophic PV inversion of conserved redistributions of the PV distribution corresponding to a motionless atmosphere. Left panel: $\delta\hat{M}$ for single layer downgradient transport of PV, with each layer being as in the left panel of Fig. 3.2. Right panel: $\delta\hat{M}$ for single layer upgradient transport of PV, with each layer being as in the left panel of Fig. 3.2.

3.4, it can be seen that $\delta\hat{M}$ is higher for lower isentropic levels. This can be attributed to the notion that the mass bounded between equally spaced (in Kelvin) isentropes, is higher for lower isentropes, as density decreases with height. Noting that potential temperature increases with height whereas pressure decreases with height, the interval of 710K to 754K falls roughly between 17.5 and 15.0 hPa. The result of this, is that the density along the isentropes shown in Fig. 3.4 decreases approximately linearly, which is reflected in the linear curve of $\delta\hat{M}$. At lower isentropic levels, a reconfiguration of PV induces the displacement of relatively more mass, giving rise to higher absolute values of $\delta\hat{M}$. The same can be said for $\delta\hat{M}$ resulting from the upgradient configurations, shown in the right panel of Fig. 3.4. There the now positive values of $\delta\hat{M}$ are higher on lower isentropic levels. The choppiness of the curves shown in Fig. 3.4, can most likely be attributed to the coarseness of the grid as well as the approximations made in calculating $\delta\hat{M}$ from the inverted fields. A notable difference between $\delta\hat{M}$ for the up and downgradient configurations, is that they are not each others opposite. Given the anti-symmetry of their respective re-distributions of PV, one might expect their respective $\delta\hat{M}$ to also be anti-symmetric. The observed disparity between the negative and positive $\delta\hat{M}$, is complicated by the physical interpretation of the upgradient configuration being less clear-cut than that of the downgradient configuration, which can 'naturally' be associated with mixing-zones. An upgradient re-configuration of PV could also be argued to be the 'inverse' of the downgradient configuration shown in the left panel of Fig. 3.2, in the sense that upgradient fluxes would restore the PV-distribution back to its initial state. The resulting $\delta\hat{M}$ would then indeed be the opposite of those resulting from the downgradient configurations. But regardless of the disparity between $\delta\hat{M}$ for the up and downgradient configurations, the character of their respective net angular momentum changes is in line with those anticipated from QG-theory.

In section 3.2, an analytical example was given of the angular momentum loss associated with downgradient transport of QGPV. In particular, it was shown that in QG-theory, the change in absolute angular momentum is proportional to $\delta M = -2/3\rho_0 H_0 \beta b^3$ (Eq. 3.2.5), where $b$ is half of the meridional extent of the anti-symmetric 'mixing-zone' shown in Fig. 3.1. This theoretical result is investigated using cyclo-geostrophic PV-inversion, with a mixing-zone as in the left

panel of Fig. 3.2. For the meridional extent of the mixing-zone, measured from its center at 50 degrees North, the parameter $\hat{b}$ is introduced to distinguishes from $b$ used in Fig. 3.1. In the left panel of Fig. 3.5, $\delta\hat{M}$ as a function of the total meridional extent ($2\hat{b}$) of the downgradient configuration, or mixing-zone, is plotted. $\delta\hat{M}$ can be seen to increase sharply as a function of

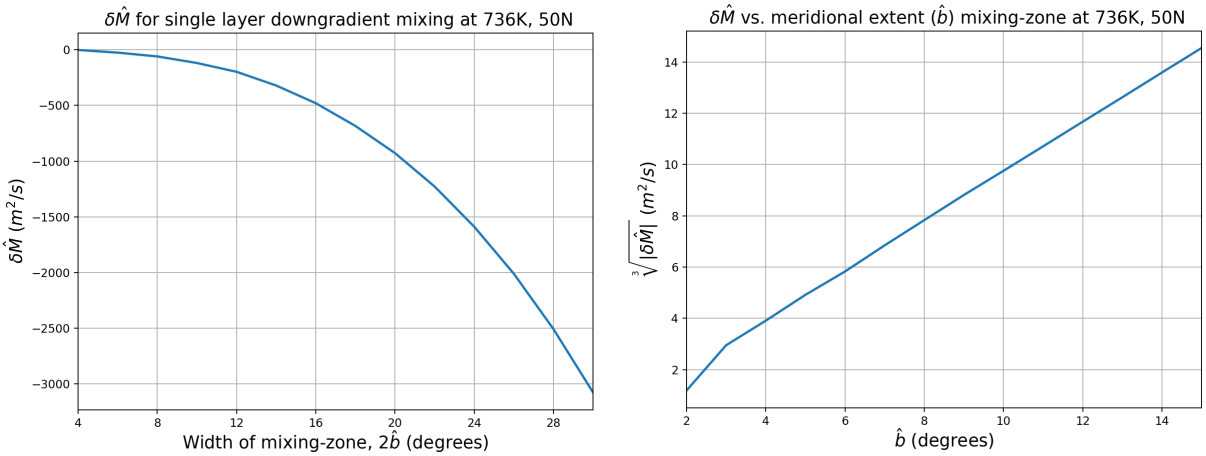


**Figure 3.5:** Change in absolute angular momentum per unit mass ($\delta\hat{M}$), as determined by cyclo-geostrophic PV inversion, for increasingly wider downgradient configurations, or 'mixing-zones' as in section 3.2. Left panel: single layer mixing-zone at 736K with meridional extent $2b$, with $b$ as in Fig. 3.1, centered around 50 degrees North. Right panel: Cube root of the absolute value of $\delta\hat{M}$, as a function of half the mixing-zone width ($b$).

the width of the mixing-zone. In the right panel of Fig. 3.5, the cube root of the absolute value of $\delta\hat{M}$ is plotted as a function of $\hat{b}$. The fact that this curve is linear, at least between $\hat{b} = 3$ and $\hat{b} = 15$ degrees, shows that $\delta\hat{M}$ is proportional to $\hat{b}^3$. This is in agreement with the quasi-geostrophic result for $\delta M$, given by Eq. 3.2.5. The deviation from the linear trend at $\hat{b} \leq 2$ degrees, could be attributed to (1) numerical issues with the coarseness of the grid and the methods used to calculate $\delta\hat{M}$, in particular with the jets not being resolved properly for small $\hat{b}$, (2) the nature of $\delta\hat{M}$ changes when $\hat{b}$ becomes smaller than the Rossby radius of deformation, where the flow shifts from geostrophic to cyclostrophic order. Although point (2) would raise interesting questions, point (1) is by far the most likely candidate, judging by the morphology of the resolved wind-fields for $\hat{b} \leq 2$ degrees (not shown here).

# Chapter 4

# Planetary wave drag in the general circulation

Planetary waves play an important role in shaping the general circulation. Not least, planetary waves are involved in driving the observed surface westerlies and wintertime stratospheric Brewer-Dobson circulation. To elucidate the role of planetary waves in the general circulation, the transfer of angular momentum by planetary waves has been parameterized in a simplified zonal mean model of the atmosphere, described in Van Delden [32]. In section 4.1, this model is used to perform model experiments. The model's parameterization of planetary waves and the model's output, will be interpreted based on the theory described in Ch. 2 and 3. In section 4.2, model performance will be quantified with the use of Taylor-diagrams. Taylor-diagrams are a graphical measure of the correspondence between the modelled and observed atmosphere, and are commonly used in climate science.

## 4.1 A simplified model of the general circulation

The model is a simplified zonal mean primitive equations model, that was constructed for the purpose of gaining insight into the fundamental dynamical processes that shape the general circulation. The model features a simplified representation of (1) the seasonal insolation cycle, (2) greenhouse gasses, namely $CO_2$, $O_3$ and $H_2O$, (3) a hydrological cycle, including an Intertropical Convergence Zone (ITCZ), (4) planetary wave drag in the stratosphere. These dynamics can be individually turned on or off, in order to study their dynamical effects on the zonal mean atmosphere. In the context of this thesis, planetary wave drag is of particular interest and will correspondingly be emphasized throughout this section. This section will be concluded with suggestions for possible improvements of the model. For a more comprehensive description of the model, the reader is referred to Van Delden [32].

A key aspect of the model is that it does not inherently support planetary waves. The model does support horizontally propagating acoustic Lamb waves, but these have negligible physical significance. In the current iteration of the model, planetary waves are instead parameterized by prescribing a retrograde 'drag' force in the wintertime stratospheric surf-zone. This parameterization is meant to capture the effect of angular momentum loss due to planetary wave breaking. The planetary wave drag ($D$) is parameterized as

$$D = D_0 B(\phi) L(z), \tag{4.1.1}$$

where

$$B(\phi) = \sin(2|\phi|) \tag{4.1.2}$$

and

$$L(z) = \begin{cases} \sin\left[\pi\left(\frac{z-z_0}{z_1-z_0}\right)\right] & \text{if } z_0 < z < z_0 \\ 0 & \text{otherwise,} \end{cases} \tag{4.1.3}$$

with $z_1 = 25\text{km}$, $z_0 = 10\text{km}$ and $D_0 = -5 \cdot 10^{-5}\ m/s^2$. In the expression for $B$, $\phi$ is the latitude coordinate in degrees. The region in which $D$ is defined roughly corresponds the shape of the wintertime stratospheric surf-zone. The parameterization of $D$ takes into account the Charney-Drazin condition for upward planetary wave propagation discussed in section 2.2, by setting $D_0 = 0$ if the zonal wind $u < 0$ at any level below the region in which $D$ would otherwise be prescribed.

Three different configurations of the model are compared against the observed climatology in Fig. 4.1. Model run 2a, shown in the top left panel of Fig. 4.1, includes only a yearly insolation

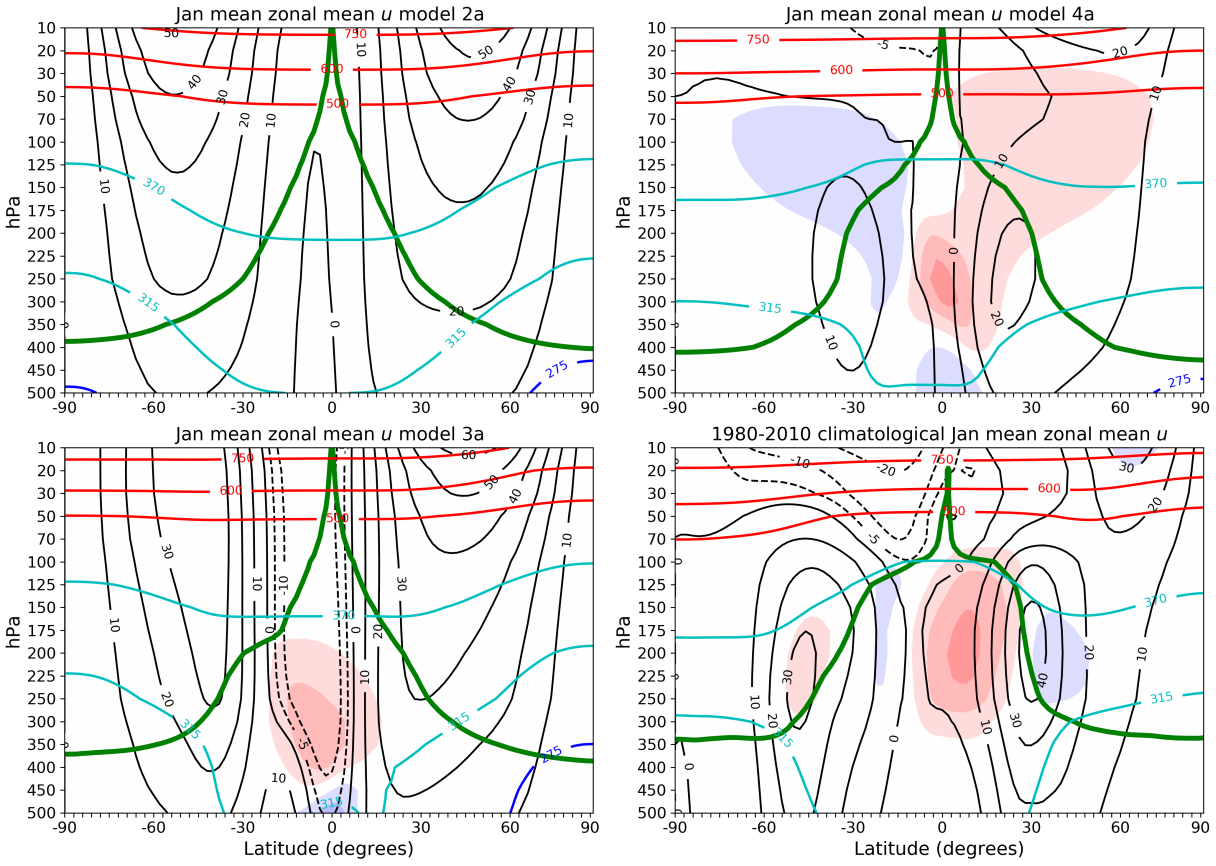


**Figure 4.1:** Comparison of model output with climatological observation for January. Model output is interpolated to ERA-Interim pressure levels. Red, magenta and blue lines mark isentropes of the over, middle and underworld, respectively. Solid black lines mark positive zonal velocities, dotted black lines negative zonal velocities. Thick green line marks the 2 PVU dynamical tropopause. Red and blue shading represent positive and negative meridional wind, respectively, with 0.5 $m/s$ spacing. Top left: Model run 2a, featuring only an insolation cycle. Bottom left: Model run 3a, featuring an insolation and hydrological cycle. Top right: Model run 4a, featuring an insolation cycle, hydrological cycle, and planetary wave drag. Bottom right: Climatological ERA-Interim observation.

cycle and longwave radiation absorption by $CO_2$. The resulting zonal mean atmosphere has

the properties that (1) the isentropes bulge downward towards the equator everywhere, (2) year round hemisphere-wide zonal jets exist on both hemispheres, (3) no significant meridional component of the wind is present, (4) the dynamical tropopause marked by the 2 PVU contour, decreases inversely with latitude and is symmetric with respect to the equator. Model run 3a, shown in the bottom left panel of Fig. 4.1, extends model 2a with the addition of a hydrological cycle and shortwave absorption by $H_2O$ and $O_3$. Differences in the model output with respect to model 2a are, (1) the hydrological cycle's transfer of energy affects the position of the isentropes of the middle and underworld, (2) updraft induced by latent heat release in the ITCZ, as well as updraft induced by the position of the Hadley cell in January, causes a reversal of the temperature gradient close to the equator, inducing westward winds there, (3) sharpening of the PV-gradient of the dynamical tropopause between 30 and 40 degrees latitude in the summer-hemisphere. Sharpening of PV-gradients is associated with an acceleration of the associated jet core (section 3.3), which alludes to a role of the ITCZ in 'driving' the subtropical jet. More specifically, that latent heat release in the ITCZ helps to maintain the strong temperature gradient, or corollary pressure gradient, which induces the subtropical jet (e.g. Persson [33]). In the winter-hemisphere of model 3a, evaporation leads to a more rapid cooling of the surface, because one-fifth of the evaporation is set to convergence into the ITCZ. This effectively makes evaporation a mechanism for equatorward energy transport. Through thermal wind balance, the corresponding increase in the temperature gradient in the winter-hemisphere induces a stronger zonal jet. Model run 4a, shown in the bottom left panel of Fig. 4.1, includes the parameterization of planetary wave drag. Notable improvements over model 3a, and also with respect to the observed climatalogical zonal mean plotted in the bottom right panel, are (1) the existence of a cold-point tropopause, created by upwelling induced by the stratospheric meridional winds which are in turn induced by planetary wave drag, (2) reversal of the stratospheric winds, with the winds now blowing westward in the summer-hemisphere, (3) separation of the hemisphere-wide yet into a subtropical and polar night jet, (4) a sharp PV-gradient along the dynamical tropopause PV-gradient between 60 and 30 degrees North and South. Some aspects of reality which are captured less well by model 4a, are (1) the magnitude and location of the meridional wind, (2) the temperature of the lower atmosphere, which is too cold, (3) magnitude of the zonal wind, with both the westward and eastward winds generally being too weak. Between model 4a and 3a, the westward winds within the equatorial region nearly completely vanish. A possible cause of this could be an increased spreading of heat by more homogeneous planetary wave drag-induced upwelling. During the winter to summertime transition, planetary wave drag brings the zonal winds close to a full stop. When the zonal winds are sufficiently weak during the onset of summer, the positive equator-to-pole temperature gradient caused by absorption of shortwave radiation by ozone, induces a westward wind through thermal wind balance. The upwelling induced by planetary wave drag, also appears to play a role in 'inverting' the temperature gradient in the upper regions of the atmosphere. Without planetary wave drag, the eastward winds are too strong for the westward 'signal' of the wind to express itself.

The parameterization of planetary wave drag given by Eq. 4.1.1, can be considered a 'metaphor' for a more complex set of interactions. Namely, a metaphor for nearly all the dynamics discussed in Ch. 2 and 3, with planetary wave breaking and the resulting planetary wave drag being only a piece of the puzzle, so to speak. Dynamics that cannot be captured by the model due to planetary waves not being resolved, are (1) the 'elasticity' of planetary waves on the sharp PV-gradient of the polar night jet (or polar vortex edge), adding to the resilience of the polar night jet, (2) a critical layer or 'surf-zone', which by itself influences the behavior of planetary waves (i.e. the surf-zone can reflect, absorb or over-reflect planetary waves), (3)

self-sharpening of the polar night jet's PV-gradient as a result of planetary wave breaking, accelerating the core of the jet and further increasing its planetary wave elasticity, (4) a source region of planetary waves, in which the zonal flow is accelerated and from which planetary waves propagate upwards into the stratosphere. The interplay between the aforementioned (planetary wave) dynamics, 'naturally' lead to the establishment of a polar night jet, or polar vortex[1]. Because the dynamics surrounding the polar night jet rely to such a large extent on the existence of planetary waves, an isolated polar night jet does not by itself appear in the model, as is evident from model 3a (bottom left panel of Fig. 4.1).

The parameterization of planetary wave drag introduced in model 4a, effectively 'pushes' the hemisphere-wide zonal jet apart into two separate jets. In the winter-hemisphere, the resulting zonal wind pattern resembles that of the subtropical and polar night jet. Separation of the otherwise hemisphere-wide yet into a subtropical and polar night jet solely by applying planetary wave drag, does however not fit in with the description of the 'wave-turbulence jigsaw puzzle'. Within the framework of the jigsaw puzzle (hereby referring to a self-sharpening jet and the dynamics discussed in Ch. 2 and 3), the resilience and self-sharpening properties of the polar night jet play an important role. They in part cause the wintertime stratosphere to efficiently organize into a jet and surf-zone (PV-)structure, with 'efficiently' referring to the amount of planetary wave breaking (or planetary wave drag) involved in maintaining a clear distinction between the low PV-gradient of the surf-zone and high PV-gradient of the polar night jet. A measure of the amount of planetary wave breaking involved in maintaining the stratosphere's PV-structure, is the strength of the meridional wind. When a westward force is applied, the atmosphere is brought out of thermal wind balance. To restore thermal wind balance, a meridional component of the wind is induced, which correspondingly weakens the temperature gradient by transporting heat polewards. In addition to this, a westward force corresponds to a converging EP-vector, which is equivalent to an equatorwards flux of (QG)PV[2] (section 3.1). As such, the zonal mean meridional component of the wind is an indirect measure of the amount of downgradient PV-mixing by breaking planetary waves. Downgradient PV-mixing in turn reduces the PV-gradient of the surf-zone and sharpens the PV-gradient of the polar night jet, and hence it helps to 'maintain' the wintertime stratospheric PV-structure. With the assumption that the polar night jet does not vary much in strength during a climatological winter month, the meridional wind becomes a measure of the amount of planetary wave breaking, or planetary wave drag.

From observation, typical zonal mean meridional winds throughout the surf-zone are on the order of 5 $cm/s$. In model 4a, shown in the top right panel of Fig. 4.1, the zonal mean meridional winds are on the order of 50 $cm/s$. That the modelled meridional wind is an order of magnitude higher than the observed wind, indicates that the real atmosphere is more efficient at organizing the otherwise hemisphere-wide jet into a subtropical and polar night jet, compared to the 'brute force' split by planetary wave drag in model 4a. In the opinion of the author, this result is in agreement with the framework set by the wave-turbulence jigsaw puzzle (in particular, that of a self-sharpening jet). Further support of this view, is that the winds of the observed subtropical

[1]The interplay between these dynamics and the resulting 'emergent' jet structure, is described in full as the 'wave-turbulence jigsaw puzzle' by McIntyre [28]. The self-organizing of a stratified and rotating fluid into 'PV-steps' (i.e. jets and mixing-zones), can also be observed in idealized model experiments, e.g. Dritschel and Scott [27][34].

[2]In isentropic coordinates, a poleward mass flux leads to dilution of PV-substance over the pole, which corresponds to an equatorward Rossby-Ertel PV-flux. With this, a (zonal mean) meridional wind can also be understood as an equatorward PV-flux, without invoking planetary wave dynamics.

and polar night jet are significantly stronger than those modelled[3]. If the parameterization of planetary wave drag is indeed less efficient at forming two separate jets, a relatively large amount of angular momentum is lost in the process, which could result in the modelled jets being weaker than the observed jets.

A 'wave-turbulence jigsaw' description of the subtropical jet is beyond the scope of this thesis. It does however seem likely that dynamics similar to that of the polar night jet apply, as the subtropical jet features (externally forced) planetary waves on a sharp PV-gradient. The observed zonal winds of the subtropical jet are higher than those modelled, which too alludes to an 'efficient' manner in which the subtropical jet is formed and sustained. It should be noted that the subtropical and polar night jet can to a certain extent be considered as two separate entities. Although the parameterization of planetary wave drag indeed splits the otherwise hemisphere-wide jet into two jets, the sharp PV-gradients that form along the surf-zone when planetary waves break in the real atmosphere, do not correspond to the sharp PV-gradients of the subtropical and polar night jet. Downgradient PV-mixing by planetary wave breaking typically occurs along isentropic surfaces, because conditions in the stratosphere are approximately adiabatic and frictionless on the timescale of planetary wave breaking events. However, the subtropical and polar night jet lie along completely separate isentropes, as is discussed in more detail in Appendix A.7.

Even though the parameterization of planetary wave drag in model 4a remains a metaphor for a broader set of interactions, model 4a does yield a qualitatively correct picture of the atmosphere's middleworld. Exceptions are the zonal winds which are too weak, and the Brewer-Dobson circulation which is too strong. But regardless, model 4a produces interesting insights, and the particular parameterization of planetary wave drag fits the framework of a simplified zonal mean model. A future model improvement could be to also include the eastward zonal force associated with planetary wave source regions. Indeed, if planetary waves are to be parameterized in the form of a body force, it would only be fair to include both the waves' positive and negative zonal forcings. A notion which supports this view, is that on average Earth's rotation speed, or angular momentum, does not change. If planetary waves are parameterized only by a westward force, this would create a persistent reduction of angular momentum of the atmosphere, and hence also of that of the Earth. Including a 'surface' eastward force whose positive torque is balanced by the negative torque in the region spanned by $D$ (Eq. 4.1.1), would perhaps be the simplest option. Such a parameterization corresponds to some extent with the parameterization scheme proposed by Hitchman and Brasseur [35], in which total planetary wave activity ($A$, Eq. 2.3.3) is conserved, with $A$ being produced in planetary wave source regions and dissipated in the 'surf-zone'. Other possible 'planetary wave' extensions, but which are not necessarily in line with the model's philosophy (i.e. they are rather complex), could be (1) a parameterization scheme in which planetary wave activity is conserved, but including the dynamics of a single resolved planetary wave, as proposed by Garcia [36], (2) a dynamical zonal mean surf-zone created by the inclusion of a single zonal harmonic, as proposed by Haynes and McIntyre [37].

[3]It could also be that the modelled zonal winds are too weak for other reasons. The model's zonal winds can be increased by decreasing the heat capacity of the surface, which causes higher temperature gradients and thus, through thermal wind balance, higher zonal velocities. For a separate subtropical and polar night jet to form, planetary wave drag ($D_0$) correspondingly has to be adjusted. If the modelled zonal winds are configured to match the order of the observed winds, the meridional winds induced by planetary wave drag are roughly 30 to 40 times larger than those observed. This effectively rules out the model's zonal winds being too weak for reasons other than having being slowed down by planetary wave drag.

## 4.2 Quantifying model performance

Taylor-diagrams, first described in a paper by Taylor [38], are an often employed method for quantifying model performance. A Taylor-diagram provides a graphical summary of how closely a modelled zonal mean pattern $r$ matches the observed zonal mean pattern $f$, where $r$ and $f$ represent the same parameter, e.g. the zonal wind. In a Taylor-diagram, the correlation coefficient $R$, centered root-mean-square difference $E'$ and standard deviation of the model $\sigma_r$ and observation $\sigma_f$, are plotted in a two-dimensional plane. This is possible because the three statistical measures are related through a geometric cosine-rule, by

$$E'^2 = \sigma_f^2 + \sigma_r^2 - 2\sigma_f\sigma_r R. \tag{4.2.1}$$

For a dataset with $N$ uniform grid-points, the correlation coefficient, centered root-mean-square error and standard deviations are calculated as

$$R = \frac{\frac{1}{N}\sum_{n=1}^{N}\left(f_n - \bar{f}\right)\left(r_n - \bar{r}\right)}{\sigma_f\sigma_r} \tag{4.2.2a}$$

$$E'^2 = \frac{1}{N}\sum_{n=1}^{N}\left[\left(f_n - \bar{f}\right) - \left(r_n - \bar{r}\right)\right]^2 \tag{4.2.2b}$$

$$\sigma_r^2 = \frac{1}{N}\sum_{n=1}^{N}\left(r_n - \bar{r}\right)^2 \tag{4.2.2c}$$

$$\sigma_f^2 = \frac{1}{N}\sum_{n=1}^{N}\left(f_n - \bar{f}\right)^2, \tag{4.2.2d}$$

where the mean of the respective fields is denoted by an overbar. Eq. 4.2.2a-4.2.2d show that the mean value of the fields is subtracted in each statistical measure, and hence Taylor-diagrams are unable to quantify an overall bias in the data.

In the context of the model experiments described in the discussion surrounding Fig. 4.1, the 'pattern' of most interest is arguably the zonal wind. This is motivated by the notion that the pattern of the zonal wind between model 3a and 4a greatly improves with respect to the observed climatology. Furthermore, following the discussion in section 4.1, the pattern of the meridional wind is expected to be unrealistic due to the manner in which planetary waves are parameterized. The pattern of the zonal mean wind is most striking during the respective wintertime months on the Northern and Southern hemisphere. During wintertime, stratospheric winds in the summer hemisphere are westward and in the winter hemisphere a subtropical and polar night jet are present. For the months January and June, the skill of the models with respect to the observed climatological zonal wind is quantified by the Taylor-diagrams shown in Fig. 4.2. In the Taylor-diagrams, the proximity of the markers for model 2a, 3a and 4a to the red dot marked 'observation', is a measure of skill of the models with respect to reproducing the observed climatological pattern of the zonal wind. It can be seen that model 3a is an improvement over model 2a, but they both perform poorly. Model 4a is a significant improvement over model 3a, in particular in terms of their correlation coefficient. The large difference between the standard deviation of model 3a and 4a, can be attributed to planetary wave drag having reduced the spread in the magnitude of the zonal wind by having reduced the strength of the eastward zonal wind. There appear to be no notable differences between the Taylor-diagrams of the Northern and Southern hemisphere wintertime month(s).

Taylor-diagrams comparing the model's respective potential temperature patterns with the observed climatology, are generally very good, in the sense that all statistical measures lie close

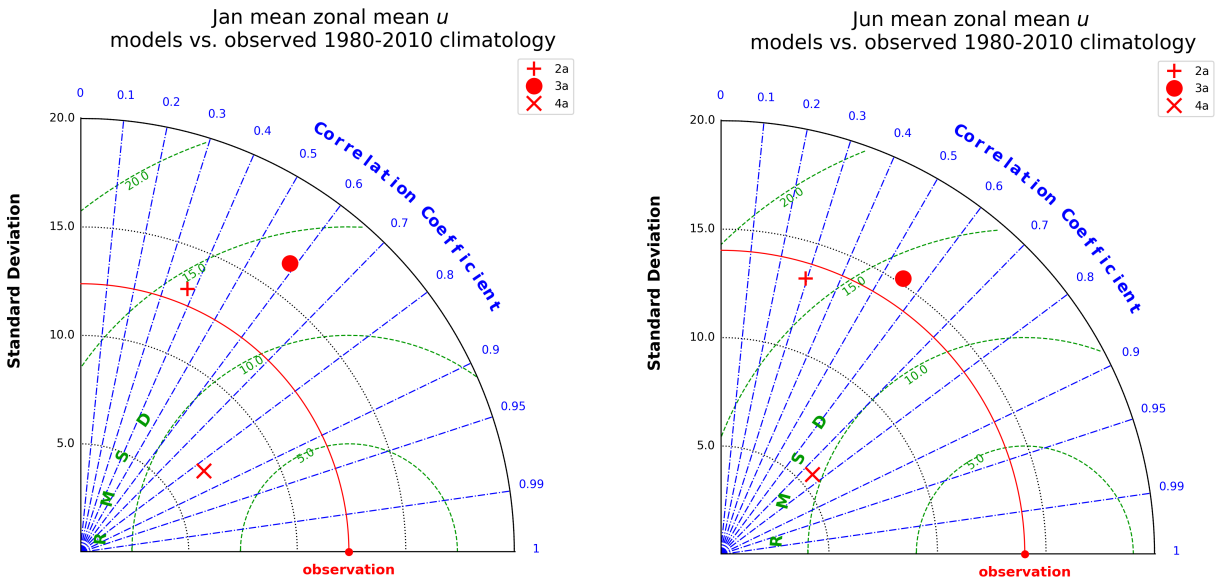


**Figure 4.2:** Taylor-diagrams comparing model 2a, 3a and 4a to the observed climatology. Left and right panel show January and June mean zonal mean zonal wind, respectively. Green, blue and grey curves mark lines of constant root-mean-square error, correlation coefficient and standard deviation, respectively. For each month of the year, Taylor-diagrams comparing the zonal wind, meridional wind and potential temperature distribution to the observed climatology are available upon request.

to observation. Although the appearance of the cold-point tropopause in model 4a is a clear improvement over model 3a, this improvement does not manifest itself in the Taylor-diagrams (not shown here). This could be attributed to the patterns of the potential temperature distribution always being in close correspondence with the observed climatology, because potential temperature increases monotonically with height. What may also play a part, is the close horizontal packing of high valued isentropes in the stratosphere, which could dominate the statistical 'signal'.

# Appendix

## A.1 Observation: ERA5 and ERA-Interim reanalysis

All observational data used within this work comes either from the ECMWF ERA5 or ERA-Interim reanalysis product. ECMWF uses extensive data assimilation system together with numerical weather prediction models, to produce a reanalysis dataset of the atmosphere, based on observations (Dee *et al.* [39]). For ERA-Interim, the dataset spans the period from 1979 until now, with data being available at 6 hourly time intervals. ERA-interim interpolates its Gaussian grid natively to a 0.75-by-0.75 degree NetCDF grid.

ERA5 is ECMWF's latest reanalysis product, which is currently in the process of being rolled out (https://www.ecmwf.int/era5). As of now, ERA5 only goes as far back as 2008, making it unsuitable for climatological analysis. Its hourly availability of data and native NetCDF grid of 0.3-by-0.3 degrees, gives it a greatly improved temporal and spatial resolution over ERA-Interim. In addition to this, a few other notable improvements over ERA-Interim are, (1) information on the quality of the data, (2) much improved troposphere, (3) improved representation of tropical cyclones, (4) better global balance of precipitation and evaporation. In the context of this thesis, the most important benefit of ERA5 over ERA-Interim, is its higher spatial and temporal resolution. This makes it possible to observe the time-development of planetary wave breaking events in high detail.

## A.2 Pseudomomentum and momentum

Following the discussion '*On the wave momentum Myth*' published by McIntyre [40], the distinction between pseudomomentum and momentum is explicitly addressed here. Pseudomomentum is a property of waves, which by definition is invariant under spatial translation of the wave in a homogeneous medium. Momentum is a vector quantity in the sense of Newton's first law. For waves in a medium, confusion can arise due to pseudomomentum often behaving 'as if' the waves themselves have momentum equal to their pseudomomentum, whereas physically, waves are associated with fluxes of momentum.

In the most general sense, momentum is a conserved quantity of a physical system under spatial translation of that system. For example, the notion of conservation of angular momentum is tied to the spatial translation of rotation. The wave property called pseudomomentum lends its name to a similar symmetry operation. Namely, that it is a conserved quantity under spatial translation of the wave in space, in a homogeneous medium. To illustrate the difference between momentum and pseudomomentum, consider a one-dimensional homogeneous rope[4] initially tied between $x = 0$ and $x = L$, carrying a disturbance as in Fig. A.3. The symmetry of this system lies in the $x$-direction. If the entire rope is displaced by a distance $\Delta x$, as in panel (a), the

[4]This example is an adaption of the 'rope dynamics' described by Stone [41].

conserved quantity under consideration is momentum. If however the rope is held fixed and only the disturbance is displaced a distance $\Delta x$, as in panel (b), the conserved quantity under consideration is pseudomomentum, given that the properties of the rope are homogeneous. If the rope would become progressively thinner towards $x = 0$, the disturbance would grow in size as it approaches this point. Spatial translation of the wave within the medium would then not be a symmetry operation, and the conservation of pseudomomentum would not apply. Put differently, if the rope is not homogeneous, a translation of the wave in space within this medium, changes the properties of the wave.

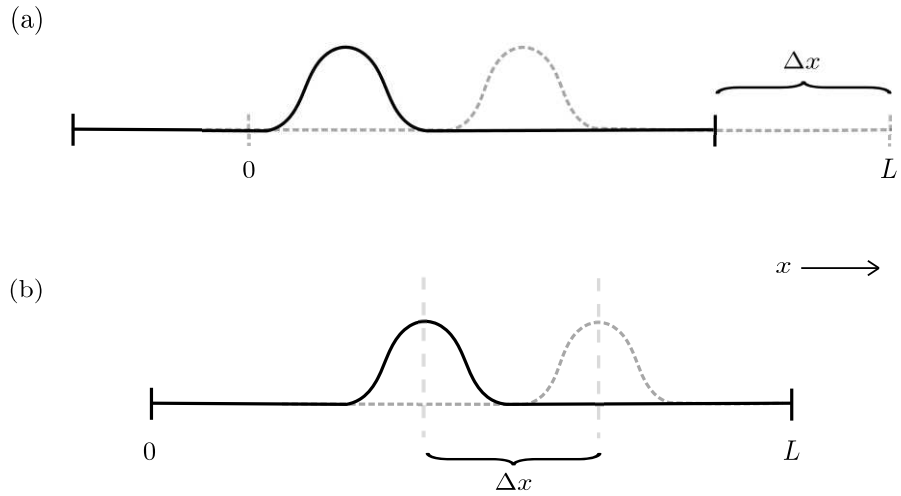


**Figure A.3:** Panel (a): Configuration of a rope initially tied between $x = 0$ and $x = L$ and carrying a disturbance (dashed line). The entire system is displaced by a distance $\Delta x$ in the negative x-direction (solid line). Panel (b): Initial configuration as in panel (a). Now the disturbance is displaced by a distance $\Delta x$, with the rope's ends fixed.

As an extension of the previous example, imagine a motionless vertically oriented metal plate being attached to the string at $x = 0$. If the disturbance from panel (b) of Fig. A.3 would propagate towards $x = 0$, it will eventually reach the plate, strike it and reflect back off it. If the plate is free to move, the impinging wave will give it a momentum impulse, and the reflected wave will be damped. If the rope is a non-dispersive medium, the incoming and reflected wave will have the same propagation speed, and thus the damping will reduce the amplitude of the wave. What results, is in an increase of momentum of the plate and decrease in pseudomomentum of the wave. For the metal plate, a change in momentum is in turn equivalent to having been subjected to a force. This thought-experiment highlights the notion that, under many circumstances, pseudomomentum determines the force when a wave interacts with matter (e.g. McIntyre [40]).

The exact description of how pseudomomentum and the momentum of the medium interact, depends on the particular problem at hand, and is often far from trivial. In the context of quasi-geostrophic planetary wave theory, the planetary wave's pseudomomentum and mean flow interaction is fully described by two equations: (1) the relation between wave induced fluxes of momentum and the mean flow is, without loss of generality, described by the Taylor-identity (section 3.1 and Appendix A.3), (2) the second-order wave-conservation law (Eq. 3.1.4), coupling the time development of zonal pseudomomentum to a zonal force. More detailed analysis of the properties of pseudomomentum, as well as examples which provide more context, can be found in Bhler [17] Ch. 4, Stone [41] and McIntyre [40]. In the context of momentum transport by geophysical waves, Vallis [2] Ch. 10 and Ch. 15 are also rich in examples.

## A.3 The Taylor-identity

In this section, the zonal mean product of $v'$ with $q'$ is derived. Here $q'$ is the quasi-geostrophic vorticity eddy term defined by the separation $q = \bar{q} + q'$, and $v'$ is the eddy component of the geostrophic meridional wind. In zonal mean form, where there are no purely zonal derivatives, the eddy term of Eq. 1.3.5a is written as

$$\overline{q'} = \overline{\frac{\partial^2 \psi'}{\partial y^2}} + \overline{\frac{\partial}{\partial z}\left(\frac{f_0 b'}{N^2}\right)}. \tag{A.3.1}$$

With the definition of $v' = \partial_x \psi'$, the multiplication of $q'$ with $v'$ follows as

$$\overline{v'q'} = \overline{\frac{\partial \psi'}{\partial x}\frac{\partial^2 \psi'}{\partial y^2}} + \overline{\frac{\partial \psi'}{\partial x}\frac{\partial}{\partial z}\left(\frac{f_0 b'}{N^2}\right)}. \tag{A.3.2}$$

Expanding the first term on the right-hand side, gives

$$\overline{\frac{\partial \psi'}{\partial x}\frac{\partial^2 \psi'}{\partial y^2}} = \overline{\frac{\partial}{\partial y}\left(\frac{\partial \psi'}{\partial x}\frac{\partial \psi'}{\partial y}\right)} - \overline{\frac{\partial \psi'}{\partial x}\frac{\partial^2 \psi'}{\partial x \partial y}} = -\frac{\partial}{\partial y}\overline{u'v'}. \tag{A.3.3}$$

Here it was used that $\overline{\partial_x \psi' \partial_{xy} \psi'} = \overline{\frac{1}{2}\partial_x(\partial_y^2 \psi')} = 0$, and that $(u', v') = (-\partial_y \psi', \partial_x \psi')$. The second term on the right-hand side of Eq. A.3.2 can be written as

$$\begin{aligned}
\overline{\frac{\partial \psi'}{\partial x}\frac{\partial}{\partial z}\left(\frac{f_0 b'}{N^2}\right)} &= \overline{\frac{\partial}{\partial z}\left(\frac{f_0 b'}{N^2}\frac{\partial \psi'}{\partial x}\right)} - \overline{\frac{\partial^2 \psi}{\partial x \partial z}\frac{f_0 b'}{N^2}} \\
&= \overline{\frac{\partial}{\partial z}\left(\frac{f_0 b'}{N^2}\frac{\partial \psi'}{\partial x}\right)} - \overline{\frac{f_0^2}{N^2}\frac{\partial}{\partial x}\left(\frac{1}{2}\frac{\partial \psi}{\partial z}\right)^2} \\
&= \frac{\partial}{\partial z}\left(\frac{f_0}{N^2}\overline{v'b'}\right).
\end{aligned} \tag{A.3.4a}$$

On the second line it was used that $\partial_z \psi = b'/f_0$ by the definition of $b'$. Inserting the expressions of Eq. A.3.4a and Eq. A.3.3 in the expression of Eq. A.3.2, yields

$$\overline{v'q'} = -\frac{\partial}{\partial y}\overline{u'v'} + \frac{\partial}{\partial z}\left(\frac{f_0}{N^2}\overline{v'b'}\right). \tag{A.3.5}$$

This expression for $\overline{v'q'}$ is equivalent to the quasi-geostrophic zonal mean divergence of the Eliassen-Palm vector, and is often referred to as the Taylor-identity. Special attention goes out to the notion that the derivation of Eq. A.3.5 required only the separation of $q$ and $v$ in a mean and eddy term. Hence no small-amplitude assumption is needed, such that the Taylor-identity is generally valid.

## A.4 Form drag

Form drag is a mechanism for the vertical transfer of momentum in a stratified fluid. It takes place through deformation of interfaces by which layers in a fluid are bound, to which the term 'form' in 'form drag' owes its existence. The deformation of interfaces gives rise to a pressure force acting upon the layer bounded by these interfaces. To derive a general zonal mean expression for form drag, consider a layer bounded by two interfaces $h_1(x, y)$ and $h_2(x, y)$ on a domain periodic in $x$ (Fig. A.4). Note that the interfaces are two-dimensional, and are hence independent of $z$. The force resulting from a pressure gradient opposes the direction of

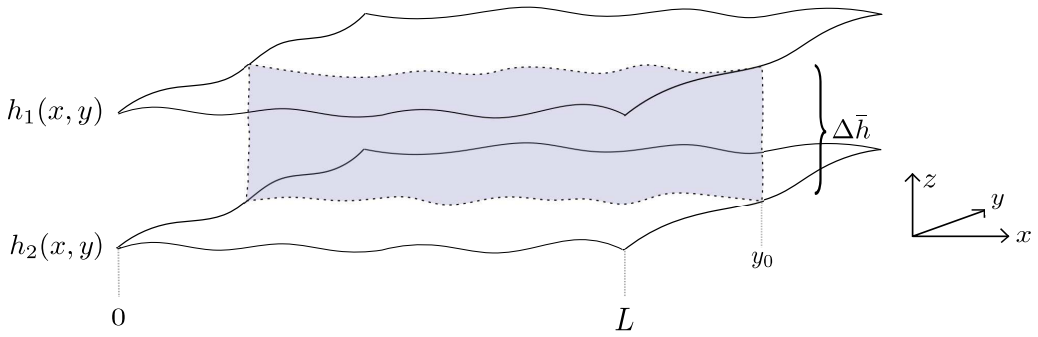


**Figure A.4:** Volume of fluid bounded by the surfaces $h_1(x, y)$ and $h_2(x, y)$, which at $y = y_0$ are separated by a mean vertical distance $\Delta\bar{h}$. The domain is periodic in $x$, and the shaded region between $x = 0$ and $x = L$ represents the area under consideration in a zonal mean analysis of form drag between the interfaces at $y_0$.

the gradient, as is evident from the equations of motion, which generally are written with a negative pressure gradient term on the right-hand side and a positive acceleration term on the left-hand side. By inspection of the shaded region in Fig. A.4, the zonal mean force resulting from the zonal pressure gradient is then given by

$$\bar{F}_x = -\frac{1}{L}\int_0^L \int_{h_2}^{h_1} \frac{\partial p}{\partial x} dx dz. \tag{A.4.1}$$

Integrating Eq. A.4.1 by parts with respect to $z$, yields the integrand

$$\int_{h_2}^{h_1} \frac{\partial p}{\partial x} dz = \left[\frac{\partial p}{\partial x} z\right]_{h_2}^{h_1} - \int_{h_2}^{h_1} \frac{\partial}{\partial z}\frac{\partial p}{\partial x} dz = \left[\frac{\partial p}{\partial x} z\right]_{h_2}^{h_1}. \tag{A.4.2}$$

Here it was used that $\partial_x \partial_z p = 0$ by hydrostasy, i.e. the vertical pressure gradient does not depend on the horizontal position within the layer. Further evaluation of Eq. A.4.1 gives

$$\bar{F}_x = -\frac{1}{L}\int_0^L \left[\frac{\partial p}{\partial x} z\right]_{h_2}^{h_1} dx = -\overline{h_1 \frac{\partial p_1}{\partial x}} + \overline{h_2 \frac{\partial p_2}{\partial x}}, \tag{A.4.3}$$

where $\partial_x p_i$ represents the zonal pressure gradient along the surface $h_i$. The terms on the right-hand side of Eq. A.4.3 are the form stresses associated with the interfaces $h_1$ and $h_2$, acting on the layer. These stress terms can be written as $\tau_1$ and $-\tau_2$, respectively, such that $\bar{F}_x = \tau_1 - \tau_2$, where $\tau_i \equiv -\overline{h_i \partial_x p_i}$. If $\tau_1$ and $\tau_2$ are not equal, there will be a momentum change within the layer due to the pressure force, to which the term 'drag' in 'form drag' refers. A pressure force, and hence form stress, is a force per unit area. $\bar{F}_x$ results from form stresses acting over a vertical distance, and it is therefore proportional to a force applied to a volume. With the mean layer depth being $\Delta\bar{h}$, it follows that per unit volume, $\bar{F}_x = (\tau_1 - \tau_2)/\Delta\bar{h}$. When the surfaces are chosen to be infinitesimally close to each other, this expression is equivalent to the definition of a derivative of $\tau_i$ with respect to $\bar{h}$. Thus for $\Delta\bar{h} \to 0$, $\bar{F}_x = \partial_{\bar{h}}\tau_i$. Noting the equivalence between $\Delta\bar{h}$ and $\Delta z$, and dropping the subscript $i$, the zonal 'form drag' force per unit volume is written as

$$\bar{F}_x = \frac{\partial \tau}{\partial z}. \tag{A.4.4}$$

Of particular interest is the quasi-geostrophic form of Eq. A.4.4. As before, $h$ refers to an interface $h(x, y)$ bounded by two layers of fluid. In quasi-geostrophic theory, $h$ as well as

pressure surfaces ($p(x, y)$) are taken to be quasi-horizontal. Using the separation $h = \bar{h} + h'$ and $p = \bar{p} + p'$, and applying quasi-geostrophic scaling to Eq. A.4.4, $\tau$ follows as

$$\tau = -\overline{h' \frac{\partial p'}{\partial x}}. \tag{A.4.5}$$

One can imagine an interface perturbation ($h'$) being proportional to a pressure perturbation ($p'$). The latter is in turn proportional to a buoyancy perturbation, or using the ideal gas law, a temperature perturbation. The next step is to formalize this relation. Consider an interface $h$ with mean value $\bar{h}$ and a buoyancy surface (or, equivalently, potential temperature surface) $b$ with mean value $\bar{b}$. These surfaces can be expressed in terms of each other to quasi-geostrophic accuracy, i.e. they can be written as $h(b)$ and $b(h)$. Using a first order Taylor expansion of $h(b)$ around $\bar{b}$, yields

$$h(b) = h(\bar{b}) + \left.\frac{\partial h}{\partial b}\right|_{b=\bar{b}} [\bar{b} - b] \approx h(\bar{b}) - \frac{\partial \bar{h}}{\partial b} b', \tag{A.4.6}$$

where it was used that $b' = b - \bar{b}$, and that to first order $\partial_b h_{b=\bar{b}} \approx \partial_b \bar{h}$. Using $h' = h(b) - h(\bar{b})$, the approximation $\partial_b \bar{h} \approx (\partial_h \bar{b})^{-1}$ and the equivalence between $\partial_h$ and $\partial_z$, Eq. A.4.6 can be written as

$$h' = -b' \left(\frac{\partial \bar{b}}{\partial z}\right)^{-1}. \tag{A.4.7}$$

In the quasi-geostrophic limit, $\partial_z \bar{b} = N^2$, where $N$ is the buoyancy frequency defined in section 1.3. Lastly, by geostrophic balance, $\partial_x p'$ is related to $v'$ through $\partial_x p' = f_0 \rho_0 v'$. Inserting the expression for $h'$ and $\partial_x p'$ in Eq. A.4.5, gives

$$\tau = \frac{f_0 \rho_0}{N^2} \overline{v' b'}. \tag{A.4.8}$$

In the analysis leading up to Eq. A.4.4, the zonal form drag per unit volume was identified as the vertical derivative of $\tau$. Taking the vertical derivative of Eq. A.4.8 and dividing by $\rho_0$ gives the quasi-geostrophic zonal 'form drag' force per unit mass,

$$\bar{F}_x = \frac{f_0}{N^2} \frac{\partial}{\partial z} \overline{v' b'} = \frac{\partial}{\partial z} \mathcal{F}^{(z)}, \tag{A.4.9}$$

where $\mathcal{F}^{(z)}$ is the vertical component of the Eliassen-Palm vector discussed in section 3.1. A buoyancy perturbation $b'$ is proportional to a negative density perturbation, but equivalently also to a positive temperature perturbation $\theta'$. From Eq. A.4.8, the poleward eddy heat flux can then be interpreted as a deformation of a pressure surface, giving rise to form stress, and corollary, vertical transport of zonal momentum. Through Eq. A.4.9, the vertical divergence of the form stress determines the local zonal forcing per unit mass. At first glance this relation might appear peculiar, but the dependence of Eq. A.4.9 on $v'$ and $b'$ is fundamentally due to geostrophic balance and the fact that a perturbation of a stratified surface is proportional to a buoyancy, or temperature, perturbation.

## A.5 PV-Gradient proof

Following the example of this proof by Andrews *et al.* [3], the vertical log-pressure coordinate $z = -H \ln(p/p_0)$ is adopted, where $H$ is the scale height and $p_0$ the surface pressure. Starting with the definition of Ertel potential vorticity $Z = \xi_a \sigma^{-1}$ (Eq. 1.4.1), a coordinate transformation

from a derivative of $Z$ in isentropic $\theta$-coordinates to one in $z$-coordinates, is applied. This is done using the identity for coordinate transformations (e.g. Charney and Stern [42], Eq. 2.28),

$$\left.\frac{\partial}{\partial s}\right|_\theta = \left.\frac{\partial}{\partial s}\right|_z - \left.\frac{\partial}{\partial s}\right|_z \theta \left(\frac{\partial \theta}{\partial z}\right)^{-1} \frac{\partial}{\partial z}, \tag{A.5.1}$$

to write:

$$\left.\frac{\partial Z}{\partial s}\right|_\theta = Z_s - \theta_s \theta_z^{-1} Z_z. \tag{A.5.2}$$

Here $s$ can be, among other parameters which span a surface, $x$ or $y$ on a $\beta$-plane. The subscripts $s$ and $z$ denote partial derivatives at constant $z$. Assuming horizontal variations in $\theta_z$ are small, such that $\theta_{zs} = 0$, the first term on the right-hand side can be written as $\theta_z (Z\theta_z^{-1})_s$. Together with the identity $(Z^{-1})_z = Z^{-2} Z_z$, Eq. A.5.2 can then be written as

$$\left.\frac{\partial Z}{\partial s}\right|_\theta = \theta_z \left(Z\theta_z^{-1}\right)_s + \theta_z^{-1} Z^2 \left(Z^{-1}\theta_s\right)_z. \tag{A.5.3}$$

Note that derivatives with respect to $s$ and $z$ are interchangeable, since they are both taken with respect to constant $z$. Per unit coordinate, density in isentropic coordinates ($\sigma$) is related to density ($\tilde{\rho}$) in $(x, y, z)$-coordinates by

$$\sigma d\theta = \tilde{\rho} dz. \tag{A.5.4}$$

Here the tilde is used to signify that $\tilde{\rho}$ represents density in log-pressure coordinates. Using Eq. A.5.4, isentropic density can to first-order be expressed as $\sigma = \tilde{\rho}\theta_z^{-1}$, and quasi-geostrophic scaling assumes small horizontal gradients, such that $\tilde{\rho} = \tilde{\rho}_0(z)$. Dropping the $z$-dependence for convenience, $Z$ can then be written as $Z = \tilde{\rho}_0^{-1}\theta_z \xi_a$. Inserting this in Eq. A.5.3, gives

$$\left.\frac{\partial Z}{\partial s}\right|_\theta = \frac{\theta_z}{\tilde{\rho}_0}\left[(\xi_a)_s + \frac{\xi_a^2}{\tilde{\rho}_0}\left(\frac{\tilde{\rho}_0 \theta_s}{\xi_a \theta_z}\right)_z\right]. \tag{A.5.5}$$

In $z$-coordinates, quasi-geostrophic potential vorticity is defined as (e.g. Andrews *et al.* [3], Eq. 3.2.15)

$$q = \xi_g + \frac{f_0}{\tilde{\rho}_0}\left(\frac{\tilde{\rho}_0 \theta_e}{\theta_{0z}}\right)_z, \tag{A.5.6}$$

where $\theta_e = \theta - \theta_0(z)$, and where $\xi_g$ is the geostrophic absolute vorticity. With the first-order approximations $\xi_a \approx f_0$, $\xi_s \approx \xi_{gs}$ and $\theta_z \approx \theta_{0z}$ (with $\theta_0$ only a function of $z$), the term in square brackets on the right-hand side of Eq. A.5.5 can be written as

$$\frac{\partial}{\partial s}\xi_g + \frac{\partial}{\partial s}\frac{f_0}{\tilde{\rho}_0}\left(\frac{\tilde{\rho}_0 \theta}{\theta_{0z}}\right)_z = \frac{\theta_z}{\tilde{\rho}_0}\frac{\partial q}{\partial s}. \tag{A.5.7}$$

Here it has been used that all terms except for $\theta$ are independent of $s$, and that $\theta_s = \theta_{es}$. The assumption $\xi_a \approx f_0$ requires that the vorticity balance is dominated by planetary vorticity. Substituting Eq. A.5.7 in Eq. A.5.5 and taking $s$ to be $y$ (the meridional coordinate in a beta-plane approximation), gives

$$\left.\frac{\partial Z}{\partial y}\right|_\theta \approx \frac{\theta_{0z}}{\tilde{\rho}_0}\left.\frac{\partial q}{\partial y}\right|_z. \tag{A.5.8}$$

In Eq. A.5.8, the left-hand side corresponds to the isentropic meridional gradient of Ertel potential vorticity and the right-hand side to a scaled isobaric meridional gradient of quasi-geostrophic potential vorticity in $z$-coordinates. The relation of Eq. A.5.8 also holds if $z$ is taken to be the Cartesian height coordinate, but then scaling factor of the QGPV-gradient will be different.

## A.6 Relating eddy fluxes of QGPV and Rossby-Ertel PV

In Appendix A.5 it was discussed how in a stratified atmosphere, the gradients of isentropic Rossby-Ertel PV ($Z$) and isobaric quasi-geostrophic PV ($q$) are related. This relationship appears to carry over to the zonal mean meridional eddy fluxes of $Z$ and $q$, as is remarked by McIntyre [43] p. 48. The relation between these two eddy fluxes of PV, alludes to the notion that by the analysis of section 3.1, isentropic zonal mean meridional eddy fluxes of $Z$ are approximately equal to (quasi-geostrophic) EP-vector divergence. Theory describing concepts equivalent to that of quasi-geostrophic EP-vector divergence, are however not worked out for isentropic Rossby-Ertel PV, at least to the author's knowledge. The numerical PV-inversion experiments in section 3.4, as well as the contents of this section, do however suggest that isentropic eddy fluxes of $Z$ play a role in the angular momentum budget similar to that of the quasi-geostrophic eddy flux term $\overline{v'q'}$. To supplement the PV-inversion experiments from 3.4, in this section, an example from observation is used to demonstrate the relation between the eddy fluxes of isentropic $Z$ and isobaric $q$.

The argument linking $Z$ to $q$ is based on the relation between their respective quasi-geostrophic gradients,

$$\left.\frac{\partial Z}{\partial y}\right|_{\theta} \approx \alpha \left.\frac{\partial q}{\partial y}\right|_{p}, \tag{A.6.1}$$

where $\alpha$ is a constant, $y$ is the meridional coordinate in a beta-plane approximation, and where the derivative of $Z$ is isentropic and the derivative of $q$ is isobaric (see Appendix A.5). The scaling arguments leading to Eq. A.6.1, require that the isentropic and isobaric surfaces are both quasi-horizontal, which suggests that the horizontal velocity fields along the isentropic and isobaric surfaces are also related. This in turn suggests that the zonal mean meridional eddy fluxes of $Z$ and $q$ are related, i.e. that $\left[v'Z'\right]_{\theta} \propto \left[v'q'\right]_{p}$, where the $\theta$ and $p$ subscripts denote the vertical coordinate. The term $\left[v'Z'\right]_{\theta}$ can be directly calculated from observation. To determine $\left[v'q'\right]_{p}$ from observation is more complicated, because $q$ is a derived quantity. In pressure coordinates, $q$ is defined by (Holton and Hakim [31] Eq. 6.25)

$$q = \frac{1}{f_0}\nabla^2\phi + f + \frac{\partial}{\partial p}\left(\frac{f_0}{\sigma}\frac{\partial \phi}{\partial p}\right), \tag{A.6.2}$$

where the interpretation of the terms on the right-hand side is equivalent to those on the right-hand side of Eq. 1.3.4a. In the expression for $q$ given by Eq. A.6.2, $1/f_0\nabla^2\phi$ is the geostrophic relative vorticity, $f$ is as in Eq. 1.3.3, $\phi$ is the geopotential height and $\sigma$ is defined by (Holton and Hakim [31] Eq. 6.13a)

$$\sigma = -\frac{RT_0}{p}\frac{d\ln\theta_0}{dp}. \tag{A.6.3}$$

In the definition of $\sigma$, $T_0(p)$ and $\theta_0(p)$ correspond to the temperature and potential temperature of the standard (reference) atmosphere, respectively. Potential temperature is defined in terms of temperature, pressure and surface pressure ($p_0$ =1000 hPa), by

$$\theta = T\left(\frac{p_0}{p}\right)^{R/c_p}. \tag{A.6.4}$$

For the observed isobaric relative vorticity fields $\xi_{obs}$, the assumption $\xi_{obs} \approx \xi_g = 1/f_0\nabla^2\phi$ is made, justified by the fact that geostrophic balance is generally a good approximation in the stratosphere. The 'stretching' term on the right-hand side of Eq. A.6.2, can be calculated using the temperature values defined by the standard atmosphere and the observed geopotential $\phi$.

In the following analysis, the terms $\left[v'q'\right]_p$ and $\left[v'Z'\right]_\theta$ will be compared along the 50 hPa isobar and 530K isentrope, using ERA5 reanalysis data. Following the definition of potential temperature, the 50 hPa isobar and 530K isentrope correspond to approximately to the same height. To determine $q$ at 50 hPa, observational data from the 30, 50 and 70 hPa is used. Within this region, the standard atmosphere temperature is constant, such that $T_0$ can be taken to be independent of $p$ in calculating $\sigma$. The expression for $q$ can then be expanded, using the definition of $\sigma$, as

$$q = \xi_g + f_0 + \beta(y - y_0) + \frac{f_0}{\sigma}\frac{\partial \phi}{\partial p}\left(\frac{1}{p} - \left(\frac{\partial \ln \theta_0}{\partial p}\right)^{-1}\frac{\partial^2 \ln \theta_0}{\partial p^2}\right) + \frac{f_0}{\sigma}\frac{\partial^2 \phi}{\partial p^2}. \tag{A.6.5}$$

The derivatives in Eq. A.6.5 are either of first or second order. Their respective (second-order accurate) central finite difference approximations, can be fully expressed in terms of three equidistant pressure levels. The finite difference expressions for the first and second-order derivatives for a parameter $x(p)$ evaluated at $p_1$, are given by

$$\left.\frac{\partial x}{\partial p}\right|_{p_1} = \frac{x_{p_0} - x_{p_2}}{2\Delta p} \tag{A.6.6a}$$

$$\left.\frac{\partial^2 x}{\partial p^2}\right|_{p_1} = \frac{x_{p_0} - 2x_{p_1} + x_{p_2}}{(\Delta p)^2}. \tag{A.6.6b}$$

With these finite difference expressions, $q$ can be evaluated at the 'middle level' ($p_1 = 50$ hPa) using measurements from the level below ($p_2 = 70$ hPa), the level above ($p_0 = 30$ hPa), and from the middle level itself.

For comparing $\overline{v'q'}_p$ and $\overline{v'Z'}_\theta$, two 3-day intervals over the course of a significant wave breaking event are chosen. The time frame of 3 days ensures that adiabatic and frictionless conditions apply. The first interval is chosen at the start of a wave breaking event occurring at 530K on the 22th of December, 2015, with the interval covering the 22th to 25th of December. The second interval is chosen at the terminating phase of that wave breaking event, covering the 27th to 30th of December, 2015. The respective eddy fluxes of PV over the two intervals are shown in Fig. A.5, including their correlation coefficients. The first phase of the wave breaking event (top panel) is marked by a bulge of positive (northward) eddy potential vorticity fluxes, centered over approximately 65 degrees North. For planetary wave breaking events, it appears to be typical that the sign of the eddy vorticity fluxes changes about halfway through the wave breaking event, as can be seen from the animation shown in Appendix A.8 Fig. A.9. This can also be observed in the bottom panel of Fig. A.5, where the eddy fluxes of PV are approximately the reverse of those in the top panel. In the terminating phase of the wave breaking event, the bulge of negative eddy fluxes is however shifted north by approximately 10 degrees. Note that the net eddy PV flux over an entire wave breaking event is negative, or downgradient (this notion is however not part of the consideration in this section). Some uncertainties related to the methods used to construct Fig. A.5, are: (1) the observed eddy fluxes of $\overline{v'Z'}_\theta$ are not constrained by quasi-geostrophic scaling, but this is however something which is assumed in the proof of Eq. A.6.1, (2) the $\beta$-plane approximation becomes progressively worse further away from $y_0$, leading to possibly erroneous values of $q$ close to the pole and equator, (3) the numerical schemes used to calculate $q$ each have at least some numerical error. With these uncertainties in mind, the link between $\overline{v'Z'}_\theta$ and $\overline{v'q'}_p$ does however still appears to be clearly demonstrated by Fig. A.5.

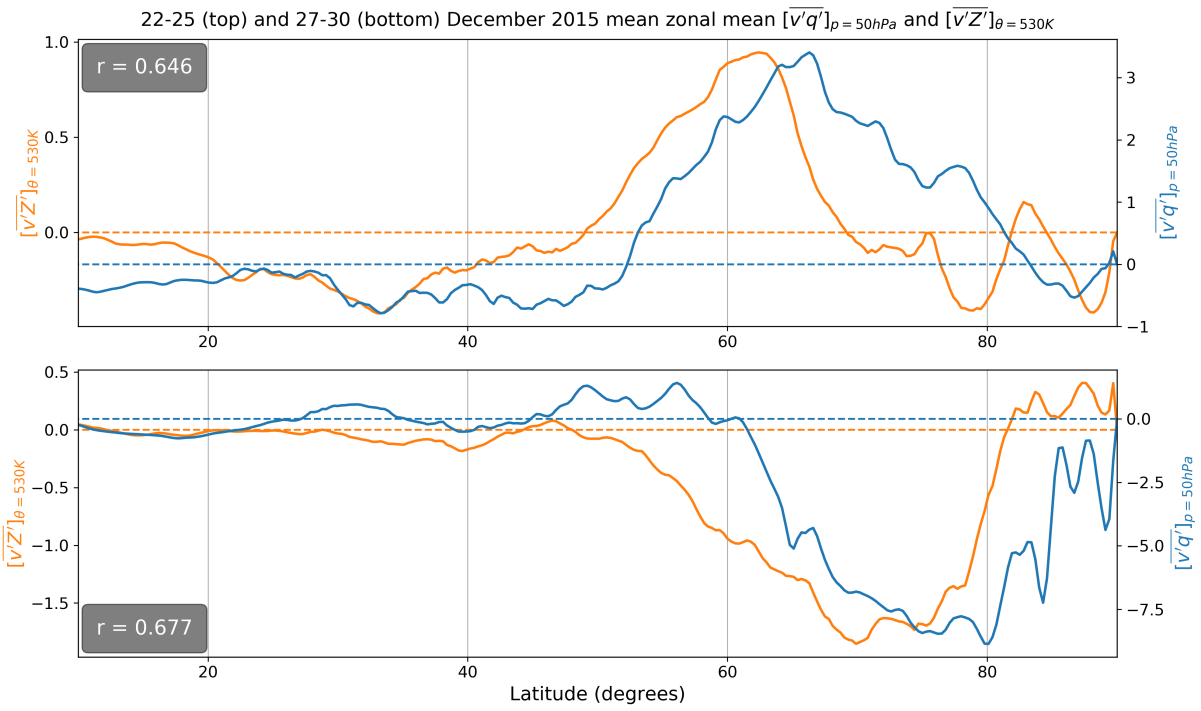


**Figure A.5:** Comparison of two 3-day mean intervals of $\overline{v'q'}_{p=50hPa}$ and $\overline{v'Z'}_{\theta=530K}$. Correlation coefficient between the two respective eddy fluxes is plotted in the top left corner of the top and bottom panels. Top panel: 22th to 25th of December '15 mean zonal mean eddy fluxes of PV. Bottom panel: 27th to 30th of December '15 mean zonal mean eddy fluxes of PV.

## A.7 PV-gradients of the subtropical and polar jet

Sharp PV-gradients can be seen to form along the edges of the idealized 'mixing-zone' shown in Fig. 3.1. Because the mixing-zone represents downgradient mixing of PV by breaking planetary waves, this might suggest that such a mixing-zone 'PV-structure' can be observed along isentropes intersecting the stratospheric surf-zone. As was mentioned in section 3.2 however, this is not the case. The diabatic processes 'driving' and the polar vortex and the resilience of the polar vortex structure, appear to play a more dominant role in shaping the stratospheric PV-gradient. This is apparent from the single sharp PV-gradient observed along the 600K isentrope and between 65 and 75 degrees North, shown in the top panel of Fig. A.6. In the lower panel of Fig. A.6, the sharp PV-gradient along the 350K isentrope and between 25 and 35 degrees North, is associated with the subtropical jet. In the middle panel of Fig. A.6, the PV-gradient along the 395K isentrope is plotted. The 395K isentrope intersects the region between the subtropical and polar night jet, as can be seen in the bottom right panel of Fig. 4.1. Correspondingly, no sharp PV-gradient is observed along the 395K isentrope. What Fig. A.6 illustrates, is that the sharp PV-gradients resulting from (isentropic) downgradient mixing of PV by breaking planetary waves, should not be associated with the sharp PV-gradients of the subtropical and polar night jet. The sharp PV-gradients of the subtropical and polar night jet do not lie along the same isentrope, and they are arguably maintained by different (diabatic) dynamics. Planetary wave breaking can however still lead to the sharpening of the PV-gradients associated with these jets.

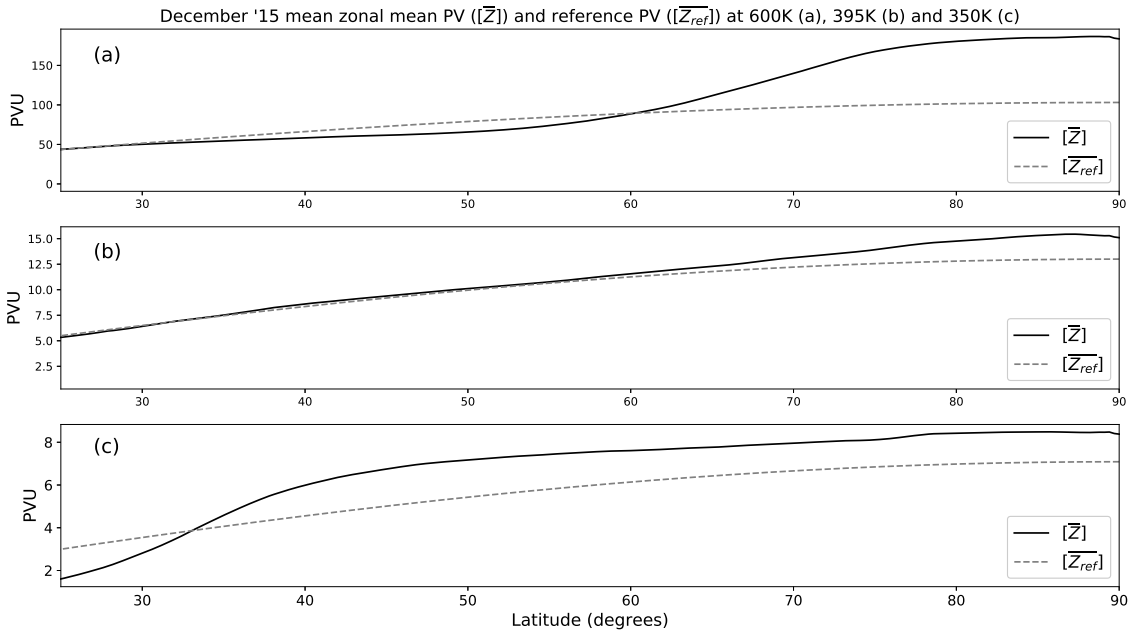


**Figure A.6:** December 2015 mean zonal mean Rossby-Ertel PV ($Z$) along the 600K (top), 395K (middle) and 350K (bottom) isentropes. Dotted grey line represents the reference PV-distribution ($Z_{\mathrm{ref}}$), corresponding to a motionless atmosphere. 1 PVU = $10^{-6}$ K m$^2$ kg$^{-1}$ s$^{-1}$. Data obtained from ECMWF ERA5 reanalysis (Appendix A.1).

## A.8 Observation: Supplementary animations

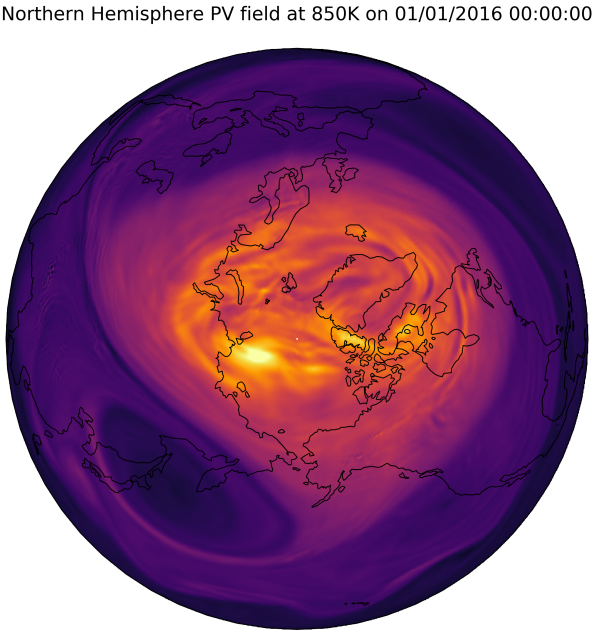


**Figure A.7:** Stereographic PV-map of the 850K isentrope, centered over the North Pole. Animations span the wintertime months (DJF). Data obtained from ECMWF ERA5 reanalysis (Appendix A.1).

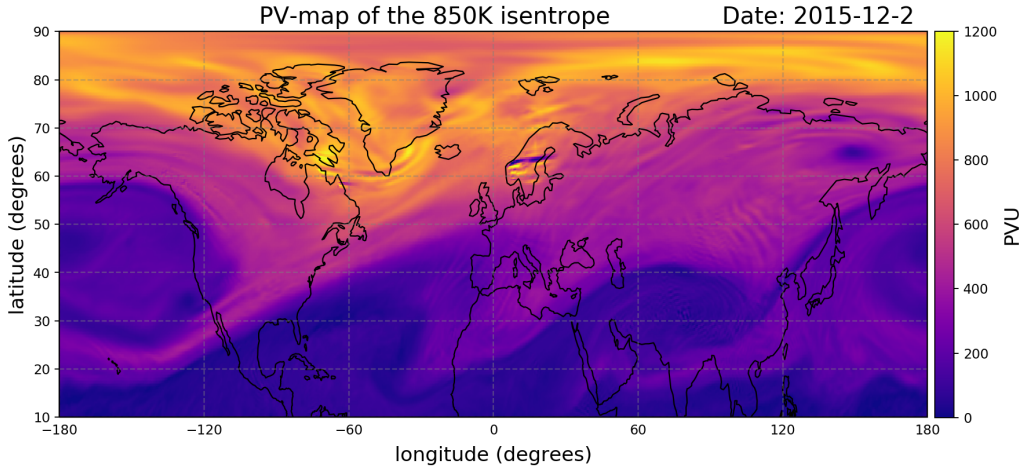


**Figure A.8:** Equirectangular PV-map of the 850K isentrope. Animations span the wintertime months (DJF). 1 PVU = $10^{-6}$ K m$^2$ kg$^{-1}$ s$^{-1}$. Data obtained from ECMWF ERA5 reanalysis (Appendix A.1).

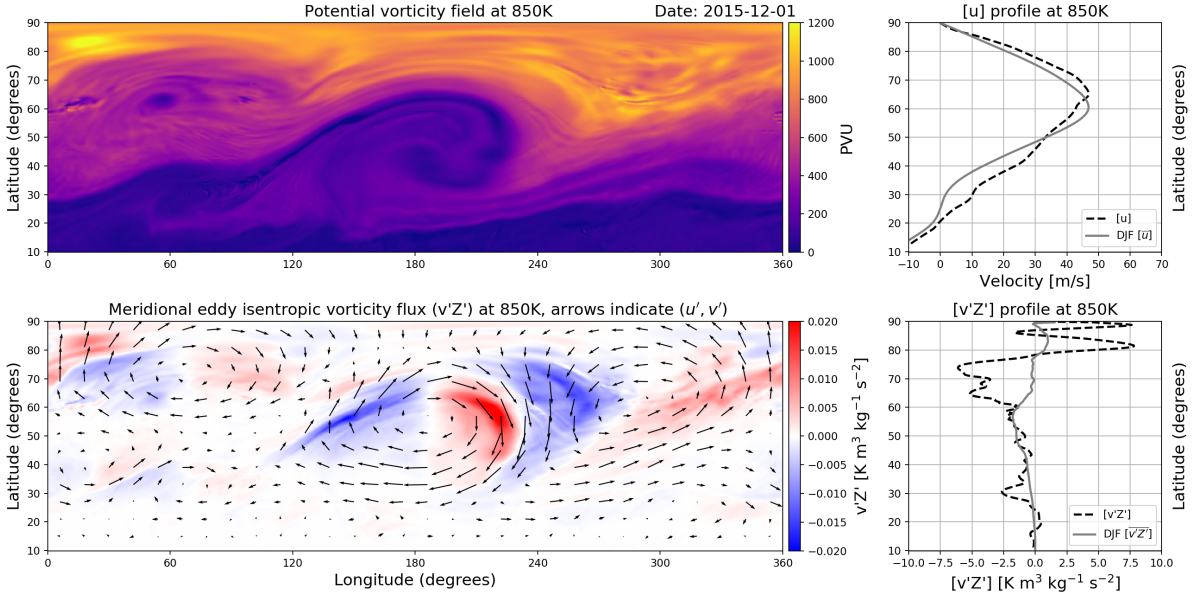


**Figure A.9:** Top left: PV-map showing the time development of the flow. Top right: Instantaneous zonal mean zonal velocity (dashed line), and DJF mean zonal mean zonal velocity (solid grey line). Bottom left: Arrows indicate instantaneous isentropic $(u', v')$ field. Red and blue shading corresponds to $v'Z'$, where $Z$ is the isentropic Rossby-Ertel PV. Bottom right: Instantaneous zonal mean $v'Z'$ (dashed line), and DJF mean zonal mean $v'Z'$ (solid grey line). Animations span the wintertime months (DJF). Data obtained from ECMWF ERA5 reanalysis (Appendix A.1).

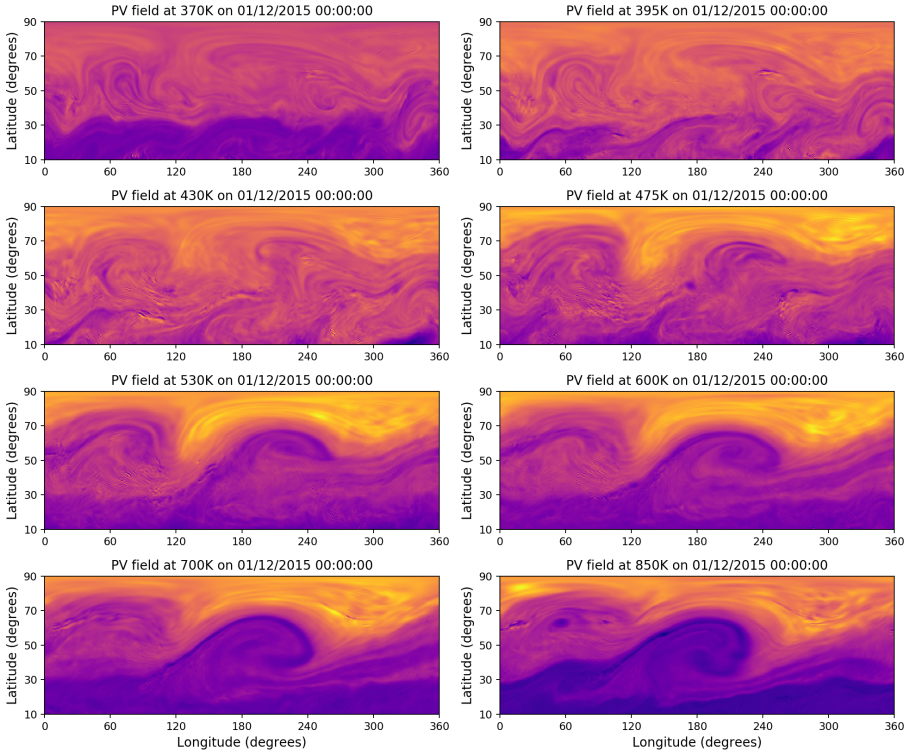


**Figure A.10:** Vertical cross-section of the atmosphere, showing the time-development of the PV-field between 370K (top left) to 850K (bottom right). Animations span the wintertime months (DJF). Data obtained from ECMWF ERA5 reanalysis (Appendix A.1).

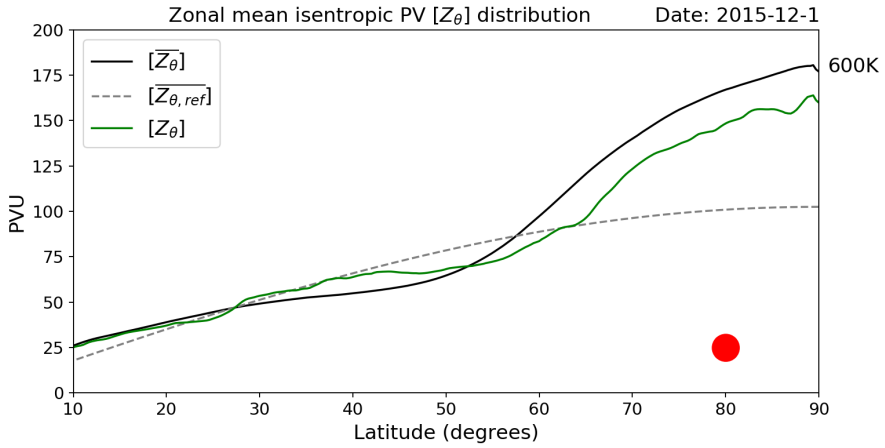


**Figure A.11:** Time-development of the zonal mean Rossby-Ertel PV ($Z$) along the 600K isentrope. Dotted grey line: Reference PV-distribution as defined in Hinssen *et al.* [30], corresponding to a motionless atmosphere. Black line: DJF zonal mean PV-distribution. Green line: Instantaneous zonal mean PV-distribution. The red dot indicates when large-scale planetary wave breaking is going on, as seen from observation. Animations available for 600K, 700K and 850K isentropes over the wintertime months (DJF). Data obtained from ECMWF ERA5 reanalysis (Appendix A.1).

# Bibliography


[1] N. Butchart, "The brewer-dobson circulation," *Reviews of geophysics*, vol. 52, no. 2, pp. 157–184, 2014.

[2] G. K. Vallis, *Atmospheric and oceanic fluid dynamics*. Cambridge University Press, 2017.

[3] D. G. Andrews, J. R. Holton, and C. B. Leovy, *Middle atmosphere dynamics*, 40. Academic press, 1987.

[4] J. R. Holton, "The role of gravity wave induced drag and diffusion in the momentum budget of the mesosphere," *Journal of the Atmospheric Sciences*, vol. 39, no. 4, pp. 791–799, 1982.

[5] B. J. Hoskins, M. McIntyre, and A. W. Robertson, "On the use and significance of isentropic potential vorticity maps," *Quarterly Journal of the Royal Meteorological Society*, vol. 111, no. 470, pp. 877–946, 1985.

[6] R. A. Plumb, "Planetary waves and the extratropical winter stratosphere," *The Stratosphere, Dynamics, Transport and Chemistry, Geophys. Monogr*, vol. 190, pp. 23–41, 2010.

[7] H. A. Dijkstra, *Dynamical oceanography*. Springer Science & Business Media, 2008.

[8] M. P. Baldwin, P. B. Rhines, H.-P. Huang, and M. E. McIntyre, "The jet-stream conundrum," *Science*, vol. 315, no. 5811, pp. 467–468, 2007.

[9] D. Dritschel and M. McIntyre, "Multiple jets as pv staircases: The phillips effect and the resilience of eddy-transport barriers," *Journal of the Atmospheric Sciences*, vol. 65, no. 3, pp. 855–874, 2008.

[10] J. G. Charney and P. G. Drazin, "Propagation of planetary-scale disturbances from the lower into the upper atmosphere," *Journal of Geophysical Research*, vol. 66, no. 1, pp. 83–109, 1961.

[11] J. Scinocca and P. Haynes, "Dynamical forcing of stratospheric planetary waves by tropospheric baroclinic eddies," *Journal of the atmospheric sciences*, vol. 55, no. 14, pp. 2361–2392, 1998.

[12] B. J. Hoskins and I. N. James, *Fluid Dynamics of the Mid-Latitude Atmosphere*. John Wiley & Sons, 2014.

[13] T. Matsuno, "Vertical propagation of stationary planetary waves in the winter northern hemisphere," *Journal of the atmospheric sciences*, vol. 27, no. 6, pp. 871–883, 1970.

[14] G. R. North, J. A. Pyle, and F. Zhang, *Encyclopedia of atmospheric sciences*. Elsevier, 2014, vol. 1.

[15] M. McIntyre and T. Shepherd, "An exact local conservation theorem for finite-amplitude disturbances to non-parallel shear flows, with remarks on hamiltonian structure and on arnol'd's stability theorems," *Journal of Fluid Mechanics*, vol. 181, pp. 527–565, 1987.

[16] M. McIntyre and T. Palmer, "The surf zone in the stratosphere," *Journal of atmospheric and terrestrial physics*, vol. 46, no. 9, pp. 825–849, 1984.

[17] O. Bhler, *Waves and mean flows*. Cambridge University Press, 2014.

[18] P. Haynes and M. McIntyre, "On the evolution of vorticity and potential vorticity in the presence of diabatic heating and frictional or other forces," *Journal of the Atmospheric Sciences*, vol. 44, no. 5, pp. 828–841, 1987.

[19] P. D. Killworth and M. E. McIntyre, "Do rossby-wave critical layers absorb, reflect, or over-reflect?" *Journal of Fluid Mechanics*, vol. 161, pp. 449–492, 1985.

[20] P. B. Rhines, "Geostrophic turbulence," *Annual Review of Fluid Mechanics*, vol. 11, no. 1, pp. 401–441, 1979.

[21] I. M. Held, "Momentum transport by quasi-geostrophic eddies," *Journal of the Atmospheric Sciences*, vol. 32, no. 7, pp. 1494–1497, 1975.

[22] D. Andrews and M. E. McIntyre, "Planetary waves in horizontal and vertical shear: The generalized eliassen-palm relation and the mean zonal acceleration," *Journal of the Atmospheric Sciences*, vol. 33, no. 11, pp. 2031–2048, 1976.

[23] H. Edmon Jr, B. Hoskins, and M. McIntyre, "Eliassen-palm cross sections for the troposphere," *Journal of the Atmospheric Sciences*, vol. 37, no. 12, pp. 2600–2616, 1980.

[24] D. G. Andrews, "On the interpretation of the eliassen-palm flux divergence," *Quarterly Journal of the Royal Meteorological Society*, vol. 113, no. 475, pp. 323–338, 1987.

[25] R. B. Wood and M. E. McIntyre, "A general theorem on angular-momentum changes due to potential vorticity mixing and on potential-energy changes due to buoyancy mixing," *Journal of the Atmospheric Sciences*, vol. 67, no. 4, pp. 1261–1274, 2010.

[26] B. J. Harvey, J. Methven, and M. H. Ambaum, "Rossby wave propagation on potential vorticity fronts with finite width," *Journal of Fluid Mechanics*, vol. 794, pp. 775–797, 2016.

[27] D. Dritschel and R. Scott, "Jet sharpening by turbulent mixing," *Philosophical Transactions of the Royal Society of London A: Mathematical, Physical and Engineering Sciences*, vol. 369, no. 1937, pp. 754–770, 2011.

[28] M. E. McIntyre, "The atmospheric wave–turbulence jigsaw," in *Rotation and Momentum Transport in Magnetized Plasmas*, World Scientific, 2015, pp. 1–43.

[29] A. J. Van Delden and Y. B. Hinssen, "Pv-$\theta$ view of the zonal mean state of the atmosphere," *Tellus A: Dynamic Meteorology and Oceanography*, vol. 64, no. 1, p. 18 710, 2012.

[30] Y. Hinssen, A. v. Delden, T. Opsteegh, and W. d. Geus, "Stratospheric impact on tropospheric winds deduced from potential vorticity inversion in relation to the arctic oscillation," *Quarterly Journal of the Royal Meteorological Society*, vol. 136, no. 646, pp. 20–29, 2010.

[31] J. R. Holton and G. J. Hakim, *An introduction to dynamic meteorology*. Academic press, 2012, vol. 88.

[32] A. J. Van Delden, "Pv-$\theta$ view of diabatic–dynamical interaction in the general circulation," *Tellus A: Dynamic Meteorology and Oceanography*, vol. 66, no. 1, p. 24 880, 2014.

[33] A. Persson, "The coriolis force and the subtropical jet stream," *Weather*, vol. 58, no. 6, pp. 244–246, 2003.

[34] R. K. Scott and D. G. Dritschel, "The structure of zonal jets in geostrophic turbulence," *Journal of Fluid Mechanics*, vol. 711, pp. 576–598, 2012.

[35] M. H. Hitchman and G. Brasseur, "Rossby wave activity in a two-dimensional model: Closure for wave driving and meridional eddy diffusivity," *Journal of Geophysical Research: Atmospheres*, vol. 93, no. D8, pp. 9405–9417, 1988.

[36] R. R. Garcia, "Parameterization of planetary wave breaking in the middle atmosphere," *Journal of the Atmospheric Sciences*, vol. 48, no. 11, pp. 1405–1419, 1991.

[37] P. Haynes and M. McIntyre, "On the representation of rossby wave critical layers and wave breaking in zonally truncated models," *Journal of the atmospheric sciences*, vol. 44, no. 17, pp. 2359–2382, 1987.

[38] K. E. Taylor, "Summarizing multiple aspects of model performance in a single diagram," *Journal of Geophysical Research: Atmospheres*, vol. 106, no. D7, pp. 7183–7192, 2001.

[39] D. P. Dee, S. Uppala, A. Simmons, P. Berrisford, P. Poli, S. Kobayashi, U. Andrae, M. Balmaseda, G. Balsamo, d. P. Bauer, *et al.*, "The era-interim reanalysis: Configuration and performance of the data assimilation system," *Quarterly Journal of the royal meteorological society*, vol. 137, no. 656, pp. 553–597, 2011.

[40] M. McIntyre, "On the wave momentummyth," *Journal of Fluid Mechanics*, vol. 106, pp. 331–347, 1981.

[41] M. Stone, "Phonons and forces: Momentum versus pseudomomentum in moving fluids," in *Artificial Black Holes*, World Scientific, 2002, pp. 335–363.

[42] J. G. Charney and M. Stern, "On the stability of internal baroclinic jets in a rotating atmosphere," *Journal of the Atmospheric Sciences*, vol. 19, no. 2, pp. 159–172, 1962.

[43] M. E. McIntyre, "How well do we understand the dynamics of stratospheric warmings?" *Journal of the Meteorological Society of Japan. Ser. II*, vol. 60, no. 1, pp. 37–65, 1982.